Little red dots as embryos of active galactic nuclei

 $\begin{array}{c} {\rm Jian-Min~Wang,}^{1,2,3} {\rm~Yi-Lin~Wang,}^{1,2} {\rm~Yong-Jie~Chen,}^4 {\rm~Jun-Rong~Liu,}^1 {\rm~Yu-Yang~Songsheng,}^1 {\rm~Cheng~Cheng,}^3 \\ {\rm~Yan-Rong~Li,}^1 {\rm~Pu~Du,}^1 {\rm~Hao~Zhang,}^{1,2} {\rm~and~Yu~Zhao}^{1,2} \end{array}$

¹Key Laboratory for Particle Astrophysics, Institute of High Energy Physics, Chinese Academy of Sciences, 19B Yuquan Road, Beijing 100049, P. R. China
²School of Astronomy and Space Science, School of Physical Sciences, University of Chinese Academy of Sciences, 19A Yuquan Road, Beijing 100049, P. R. China
³National Astronomical Observatories of China, Chinese Academy of Sciences, 20A Datun Road, Beijing 100020, P. R. China
⁴Technology and Engineering Center for Space Utilization, Chinese Academy of Sciences, Beijing 100094, P. R. China

ABSTRACT

As an unprecedented large population in the early universe, the JWST-discovered little red dots (LRDs) have garnered much attention for formation of massive black holes and galaxies, but their nature remains a mystery. The LRDs appearing as "Chimeras" like both active galactic nuclei (AGNs) and galaxies have stimulated renewed interest in the roadmap of central massive black hole (cMBH) formation in AGNs. In this paper, we suggest that the LRDs contain $M_{\bullet} \lesssim 10^6 \, M_{\odot}$ cMBHs as demonstrated by the Soltan argument and there is a large population of stellar-mass black holes (sMBHs with total mass of $\mathcal{M}_{m_{\bullet}}$) embedded inside cMBH accretion disks (cMBH-disk) as motivated by anomalous reverberations of broad H β line in local AGNs. This embryo structure of LRDs ($M_{\bullet} < \mathcal{M}_{m_{\bullet}}$) is formed as a consequence of gravitational collapse of primordial clouds. In this Chimera, accretion onto sMBHs powers the rest-frame optical continuum of the LRDs but the UV continuum is jointly contributed by slim parts of the cMBH-disks and nuclear starbursts in the core of collapsing clouds governing the appearance of the observed V-shaped spectral energy distributions (SEDs). Outflowing clumped-envelopes are unavoidably formed by radiation pressure leading to absorption features of the Balmer lines. The present model works very well for LRDs' SEDs and avoids the issues of overly massive cMBHs. Evolution of LRDs is briefly discussed including gravitational waves.

Keywords: Active galactic nuclei (16); Galaxy formation (595); High-redshift galaxies (734); Supermassive black holes (1663)

1. INTRODUCTION

The unusual features of the LRDs (Labbé et al. 2023; Maiolino et al. 2024a; Matthee et al. 2024; Kokorev et al. 2024; Kocevski et al. 2025) challenge several fundamental aspects, and have prompted a dramatic wave of various explanations for them (see a brief summary in §5). The prominent observational characteristics of the LRDs are summarized here. They are: 1) the optical spectra are extremely red, but a turnover of UV continuum appears in rest frame (Labbé et al. 2023; Greene et al. 2024) at a rough constant frequency (in agreement with the Balmer break, i.e., Setton et al. 2024). This feature, known as the V-shaped continuum, is commonly accompanied by a blueshifted trough in the spectra, referred to as the absorption profile (except for Abell 2744-QSO1 with redshift trough, see Ji et al. 2025a). In particular, the UV continuum is not simple version of star formation in the early universe (Wang et al. 2024); 2) their sizes are extremely small ($\lesssim 0.1 \sim 0.2 \,\mathrm{kpc}$) (Baggen et al. 2023); 3) the abundances are almost $100 \sim 2300$ times that of AGNs in the early universe (Pizzati et al. 2025; Ma et al. 2025); 4) extremely low X-ray emissions (Yue et al. 2024; Ananna et al. 2024); 5) non-variable fluxes over the observed bands (Zhang et al. 2024; Tee et al. 2025); 6) the cMBHs are so massive that they deviate from the well-known Magorrian relation by a factor of ~ 100 if the masses are estimated using the normal AGN scaling relation (Eq. A1 in Appendix A) (Maiolino et al. 2024b; Li et al. 2025); 7) the LRDs break down the well-known Soltan argument if they are really massive (see § 2); 8) the number density of the LRDs rapidly declines after z = 3 - 4, and peaks roughly at z = 4 - 6, preceding the peak of the star formation history by $\Delta t \sim 10^8$ yr (Zhuang et al. 2025); 9) it has been found (Ma et al. 2025) that the LRDs have a sharp cutoff in luminosity around $L_{5100} \sim 2.5 \times 10^{44} \, \mathrm{erg \ s^{-1}}$, ruling out the possibility that LRDs are the counterparts of quasars. All these properties seem diverse, but it necessitates a theoretical model for a unified explanation. However, it is not trivial to construct such a model in light of current understanding of AGNs and galaxies.

The LRDs look like AGNs because broad emission lines dominate and they (a sample of 99 LRDs) are located in AGN regions in the BPT diagram (Rinaldi et al. 2024; Zhang et al. 2025b). It has been shown that $H\alpha$ emissions are few factors brighter than normal AGNs (Hviding et al. 2025), and that they are less clustered than galaxies (Carranza-Escudero et al. 2025). Moreover, the brightest LRD recently discovered implies that LRDs are not the counterpart of quasars (Ma et al. 2025). Thus the LRDs with distinctive SEDs are not the canonical version of AGNs. On the other hand, the LRDs are less likely to be mere galaxies because the shape of the rest-frame UV continuum is different from typical high-z star forming galaxies (much flattened in LRDs, see Fig. 3 in Pérez-González et al. 2024; Taylor et al. 2025). As the astronomical version of the "Chimeras", the LRDs may actually "take" some parts of key ingredients of AGNs and galaxies to form their special structures in the early universe. These Chimeras mostly appearing in the early universe ($z \gtrsim 3 \sim 4$) motivate us to think about the fates of collapsing primordial clouds (CPCs: Hoyle 1953; Hunter 1962; Field 1964) along the roadmap of formation of cMBHs in quasars (Rees 1984). It has been realized that the origin of the rest-frame optical continuum is a matter of intense debate whether it is powered by AGNs, stars or a mixture of both (Wang et al. 2024), even something completely new.

In this paper, we will focus on the issues related to the continuum. The Soltan argument is briefly discussed for the central massive black holes in § 2. Motivated by anomalous reverberations of broad-line regions in the quasar PHL 1092 (Wang et al. 2025a, see a brief explanation in Appendix B), we suggest a model in § 3 that the accretion disk of the cMBH contains a large population of stellar mass black holes (sMBHs). The joint contributions from accretion onto both the sMBHs and the cMBH generate the V-shape spectral energy distributions (SEDs) in the LRDs. We find that the present model of cMBH-disk works quite well for the LRDs in § 4. Discussions on current models of the LRDs are provided in § 5, and other issues relating to the cosmic evolution of the proposed scenarios will be addressed in future work. We draw conclusions in the last section.

2. A CRISIS OF THE SOŁTAN ARGUMENT

First, the overabundance of the LRDs breaks down the well-known Soltan argument for accretion growth of SMBHs over cosmic time (Soltan 1982; Yu & Tremaine 2002) if the cMBH masses of LRD are estimated by Eq. (A1). Given the luminosity functions of quasars and LRDs by $\Phi_{\rm QSO}(L_{\rm Bol},z)$ and $\Phi_{\rm LRD}(L_{\rm Bol},z)$, respectively, we have the Soltan argument given by

$$\rho_{\rm acc}(z=0) = \int_0^\infty \left(\frac{\mathrm{d}t}{\mathrm{d}z}\right) \mathrm{d}z \int_0^\infty \Phi_{\rm QSO}\left(\frac{L_{\rm Bol}}{\eta_{\bullet}c^2}\right) \mathrm{d}L_{\rm Bol} + \int_0^\infty \left(\frac{\mathrm{d}t}{\mathrm{d}z}\right) \mathrm{d}z \int_0^\infty \Phi_{\rm LRD}\left(\frac{L_{\rm Bol}}{\eta_{\bullet}c^2}\right) \mathrm{d}L_{\rm Bol},\tag{1}$$

where t is the cosmic time, η_{\bullet} is the radiation efficiency (for $\eta_{\bullet} \approx 0.1$), $L_{\rm Bol}$ is the bolometric luminosity of AGNs, and c is the speed of light. It has been found that $\rho_{\rm acc}(z=0)=\rho_{\bullet}(z=0)$, where $\rho_{\bullet}(z=0)$ is the mass density of SMBHs in local galaxies (Yu & Tremaine 2002; Marconi et al. 2004). However, including the LRDs with luminosity function $\Phi_{\rm LRD} \approx \zeta_z \times \Phi_{\rm QSO}(L_{\rm Bol}, z\approx 4\sim 8)$ with a cutoff around $z=3\sim 4$ leads to a severe tension with the Soltan argument (Inayoshi & Ichikawa 2024; Jahnke 2025). Moreover, we have the mean masses of SMBHs due to accretion

$$\langle M_{\bullet} \rangle = \frac{\int \left(\frac{\mathrm{d}t}{\mathrm{d}z}\right) \mathrm{d}z \int \dot{M}_{\mathrm{acc}} \Phi(z, L_{\mathrm{Bol}}) \mathrm{d}L_{\mathrm{Bol}}}{\int \mathrm{d}z \int \Phi(z, L_{\mathrm{Bol}}) \mathrm{d}L_{\mathrm{Bol}}}, \quad \dot{M}_{\mathrm{acc}} = \frac{L_{\mathrm{Bol}}}{\eta_{\bullet} c^2}, \tag{2}$$

yielding

$$\langle M_{\bullet} \rangle_{G} \int \Phi_{G}(z=0,L) dL = (\langle M_{\bullet} \rangle_{QSO} + \zeta_{z} \langle M_{\bullet} \rangle_{LRD}) \int dz \int \Phi_{QSO}(L_{Bol},z) dL_{Bol},$$
 (3)

where $\langle M_{\bullet} \rangle_{\rm G}$ is the mean masses of SMBHs in local normal galaxies and $\Phi_{\rm G}(z=0,L)$ is their luminosity function. In principle, the relation $\int \Phi_{\rm G}(z=0,L) {\rm d}L = \int {\rm d}z \int \Phi_{\rm QSO}(L_{\rm Bol},z) {\rm d}L_{\rm Bol}$ holds since all galaxies are from evolved quasars, and we have

$$\langle M_{\bullet} \rangle_{\rm G} = \langle M_{\bullet} \rangle_{\rm QSO} + \zeta_z \langle M_{\bullet} \rangle_{\rm LRD}.$$
 (4)

Obviously, the Soltan crisis arises, namely $\langle M_{\bullet} \rangle_{\rm G} \ll \langle M_{\bullet} \rangle_{\rm QSO} + \zeta_z \langle M_{\bullet} \rangle_{\rm LRD} \approx \zeta_z \langle M_{\bullet} \rangle_{\rm QSO}$ if $\langle M_{\bullet} \rangle_{\rm LRD} \sim \langle M_{\bullet} \rangle_{\rm QSO}$ from Eq. (A1).

On the other hand, Eq. (4) yields

$$\langle M_{\bullet} \rangle_{\text{LRD}} = \zeta_z^{-1} \delta \langle M_{\bullet} \rangle \lesssim 10^6 \, \zeta_2^{-1} \delta \langle M_{\bullet} \rangle_8 \, M_{\odot},$$
 (5)

where $\delta\langle M_{\bullet}\rangle = \langle M_{\bullet}\rangle_{\rm G} - \langle M_{\bullet}\rangle_{\rm QSO}$ represents the fluctuations of mass estimations of supermassive black holes (SMBHs), $\langle M_{\bullet}\rangle_{\rm G}$ and $\langle M_{\bullet}\rangle_{\rm QSO}$ are the mean masses of SMBHs in local galaxies and quasars, respectively, $\zeta_2 = \zeta_z/10^2$ and $\delta\langle M_{\bullet}\rangle_{\rm 8} = \zeta_z/10^2$

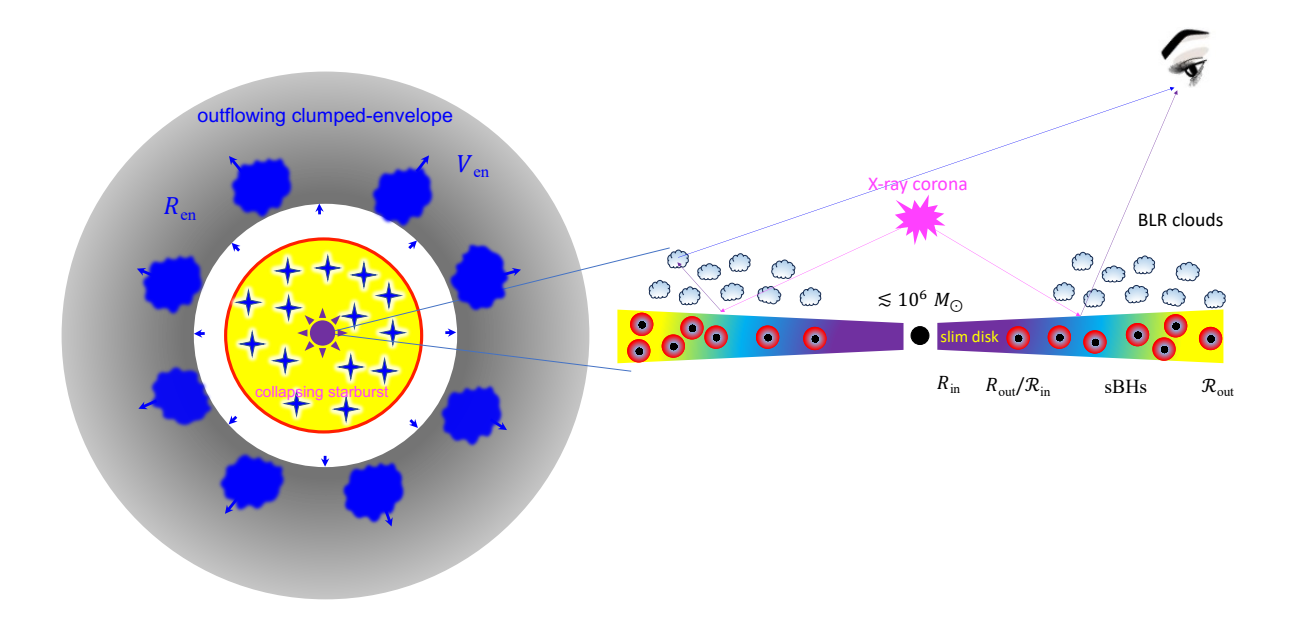


Figure 1. Structures of the LRDs formed during the collapse of primordial cloud proposed in this paper. The clumped-envelope covers the system composed of the BLR and the cMBH-disk system contributing the V-shaped SEDs of the LRDs. The cMBH-disk consists of two parts: 1) the slim disk of the central massive black hole (between $R_{\rm in}$ and $R_{\rm out}$); and 2) s@cMBH-disk represented by the part between $\mathcal{R}_{\rm in}$ and $\mathcal{R}_{\rm out}$ embedding a population of stellar-mass black holes. Since the cMBHs are not significantly smaller than normal AGNs, the s@cMBH-disk system refers to an embryo of AGNs. Given the current mass density of a collapsing primordial clouds ($\rho_{\rm c} \sim 10^{-19}\,{\rm g\,cm^{-3}}$), an outflowing clumped-envelope is formed with a typical velocity of $\sim 100\,{\rm km\,s^{-1}}$ by the radiation pressure, and has an optical depth of $\tau_{\rm abs} \approx 0.1-0.2$, explaining the absorption features when the clumps are on the line-of-sight.

 $\delta\langle M_{\bullet}\rangle/10^8~M_{\odot}$. Given the fluctuations in both galaxies and AGNs, $\delta\langle M_{\bullet}\rangle\sim\langle M_{\bullet}\rangle_{\rm QSO}$ holds. It has been found that $\zeta_z\approx 10^2\sim 10^3$ in Pizzati et al. (2025) and Ma et al. (2025). We should note that Eq. (5) is the minimum requirement to satisfy the Soltan argument, otherwise, the Soltan crisis obviously arises, namely, the accretion masses as the origin of SMBH masses will be much higher than those of local SMBHs. Therefore, the $\lesssim 10^6~M_{\odot}$ cMBHs greatly reduce the significant deviations of LRDs from the local Magorrian relation (Maiolino et al. 2024b). The issue of overmassive cMBHs as a paradox can be explained.

This, however, raises another question of what is powering the observed rest-frame optical luminosity of LRDs greatly exceeding the Eddington luminosity of the $\lesssim 10^6\,M_\odot$ cMBH accretion. Motivated by the case of PHL 1092 discussed in Appendix B, the cMBH-disk contains a population of sMBHs, which is denoted by the s@cMBH-disk system hereafter. In the LRDs, the total mass of sMBHs ($\mathcal{M}_{m_{\bullet}}$) dominates over that of the cMBH (M_{\bullet}), namely, $\mathcal{M}_{m_{\bullet}} \gtrsim M_{\bullet}$; the cMBH is still fast growing in the "womb", and this structure is thereby named the embryos of AGNs. Accretion onto sMBHs powers the rest-frame optical continuum of the LRDs, while the rest-frame UV continuum is powered by super-Eddington accretion onto the cMBHs (slim disks), nuclear starbursts of the CPCs, or a combination thereof. Fig. 1 shows the structures of the LRDs suggested in this paper.

3. cMBH-DISK AND V-SHAPED SEDS

3.1. The model

The roadmap of cMBH formation known as the Rees' diagram (Rees 1984) is very motivating in the context of collapsing primordial cloud (Hoyle 1953; Hunter 1962; Field 1964) so that we have to re-consider the fates of primordial clouds whether they can evolve into LRDs along with the roadmap of the diagram (Cenci & Habouzit 2025; Kritos & Silk 2025). Spin angular momentum (SAM) of the clouds is induced by tidal interaction with neighbors, and they acquire a dimensionless SAM of $\lambda_{\rm L} = \mathcal{J}|E_{\rm c}|^{1/2}G^{-1}M_{\rm c}^{-5/2}\approx 0.1$ if the cloud is approximated by a rigid body (Peebles 1969; Barnes & Efstathiou 1987), where \mathcal{J} is the cloud's SAM, $M_{\rm c}$ is the cloud mass, G is the gravitational constant and $E_{\rm c}$ is the total energy. However, the Compton drag due to cosmic background photons will efficiently remove the SAM ($\lambda_{\rm L} \lesssim 10^{-3}$) to form cMBHs in quasars (Loeb 1993) and a massive gaseous disk at a scale of parsecs (Eisenstein & Loeb 1995; Choi et al. 2013).

In core regions of the CPCs, a gaseous disk is formed since the primordial clouds have their own SAM. The disk radius is determined by the SAM, with $R_{\rm disk} \approx 2^{-1/2} \lambda_{\rm L} R_{\rm vir} = 4.2 \, \lambda_{\bar{3}} R_{\rm 6kpc}$ pc (Volonteri & Rees 2005), where $\lambda_{\bar{3}} = \lambda_{\rm L}/10^{-3}$ is the resultant

Table 1. Parameters of the s@cMBH-disk

cMBH-disk		Notes
M_{ullet}	 cMBH masses	$\lesssim 10^6 M_{\odot}$
\dot{M}_{ullet}^{0}	 accretion rates of the cMBH at $\mathcal{R}_{\mathrm{out}}$	$\sim 0.1 M_{\odot} {\rm yr}^{-1}$
α	 viscose parameters (keeps a constant in fitting)	0.1
$R_{ m in}$	 radius of the inner boundary of the slim disk	$3R_{ m g}$
$R_{ m out}$	 radius of the outer boundary of the slim disk ($R_{\mathrm{out}} = \mathcal{R}_{\mathrm{in}}$)	$\sim 10^5R_{ m g}$
$\mathcal{R}_{ ext{in}}$	 radius of the inner boundary of the cMBH-disk	$\sim 10^5 R_{ m g}$
$\mathcal{R}_{ ext{out}}$	 radius of the outer boundary of the cMBH-disk	$\sim 10^6R_{ m g}$
sMBHs		
m_{ullet}^0	 sMBH masses at $\mathcal{R}_{\mathrm{out}}$, i.e., $m_{\bullet} = m_{\bullet}^{0} \left(R / \mathcal{R}_{\mathrm{out}} \right)^{\beta_{\bullet}}$	$\sim 1 M_{\odot}$
Σ^0_ullet	 surface number density of sMBHs at \mathcal{R}_{out} , i.e., $\Sigma_{\bullet} = \Sigma_{\bullet}^{0} (R/\mathcal{R}_{\text{out}})^{\gamma_{\bullet}}$	$\sim 10^3\mathrm{ltd}^{-2}$
β_{ullet}	 index of sMBH mass growth migrating inward	-0.5
γ_ullet	 index of surface number density (Σ_{\bullet}) of sMBHs	0.5
ℓ_0	 factor of the saturated luminosity	$1 \sim 10$
\mathscr{M}_{mullet}	 total masses of sMBHs	$\sim 10^6M_{\odot}$
Nuclear starburst		
α_0	 normalization of NSB fluxes	$\sim 10^{7}$
t_0	 NSB ages	$0.1-0.5\mathrm{Gyr}$
Z	 NSB metallicity (keeps a constant in fitting)	$1Z_{\odot}$

SAM (after interaction with CMB) and $R_{6\mathrm{kpc}} = R_{\mathrm{vir}}/6\,\mathrm{kpc}$. Here, $R_{\mathrm{vir}} = 6.6\,\left(M_{\mathrm{H}}/10^{10}h_{0.7}M_{\odot}\right)^{1/3}\,[(1+z)/7]^{-1}\,h_{0.7}^{-1}\,\mathrm{kpc}$ (Barkana & Loeb 2001) is the virial radius of dark matter halo, M_{H} is the dark matter halo mass and $h_{0.7}$ is the Hubble constant in units of $70\,\mathrm{km\,s^{-1}\,Mpc^{-1}}$. Star formation takes place in such a gaseous disk (Chen et al. 2024, 2025b), which has been studied to explain the relation between accretion rates and star formation (Chen et al. 2009; Netzer 2009) and the metallicity of AGNs (Wang et al. 2010, 2011, 2012, 2023b; Fan & Wu 2023). Consequently, sMBHs evolved from massive stars remain inside of the accretion disks, which were originally realized as seed black holes by Eisenstein & Loeb (1995). Despite the early recognition of these seeds more than three decades ago, their roles in the structure formation of nuclear regions and observational effects have long been overlooked. If such an s@cMBH-disk system exists in AGNs, it yields anomalous reverberation of broad H β line with respect to the varying continuum. Actually, this structure could have been detected in the local quasar PHL 1092 (Wang et al. 2025a) from the long-term SEAMBH campaign (see Appendix B for details). Meanwhile, there is growing evidence for the presence of these black holes from LIGO gravitational wave detections and quasi-periodic ejections (QPEs) observed in X-rays (see discussions in Appendix C).

Moreover, the CPCs unavoidably undergo starbursts in the central region, forming a nuclear star cluster (Neumayer et al. 2020) similar to the inside-out mode in galaxies, and the cluster grows (Neumayer et al. 2020; Kritos & Silk 2025). However, details of starbursts depend on the initial density profile of the cloud and the initial mass function of the star formation (Abel et al. 2000, 2002) as well as the observational appearance of the CPC core (Kritos & Silk 2025). It is far beyond the scope of this paper to self-consistently treat the nuclear starbursts (NSBs), but we include this component to fit the LRD continuum through CIGALE.

Accordingly, the observed SEDs of the s@cMBH-disk and nuclear starbursts are determined by

$$F_{\lambda}^{c} = F_{\lambda, \text{AMS}} + F_{\lambda, \text{MBH}} + F_{\lambda, \text{NSB}}, \tag{6}$$

which are explained subsequently. First, $F_{\lambda, \mathrm{AMS}}$ is from the accreting sMBHs embedded inside the cMBH-disk, i.e., the s@cMBH-disk is the part between $(\mathcal{R}_{\mathrm{in}}, \mathcal{R}_{\mathrm{out}})$ and contributes the rest-frame optical continuum of the SEDs looking like a reddened AGN continuum. Here the subscript AMS refers to accretion-modified stars (Wang et al. 2021a), i.e., accreting sMBHs. Second, $F_{\lambda, \mathrm{MBH}}$, which is from the regions between $(R_{\mathrm{in}}, R_{\mathrm{out}})$, is responsible for ionizing the BLR for the broad Balmer emission lines. Third, $F_{\lambda, \mathrm{NSB}}$ is from a stellar component of nuclear starbursts (NSBs) (Kritos & Silk 2025), but it might also partially originate from the s@cMBH-disk. The observed Balmer break (Setton et al. 2024) corresponds to post starbursts in the nuclear regions. We would point out that $F_{\lambda, \mathrm{AMS}}$ has never been considered before as the origin of the rest-frame optical continuum of the LRDs. As a remarkable component, the presence of $F_{\lambda, \mathrm{AMS}}$ makes the LRDs neither like a pure AGN nor a galaxy, appearing as a Chimera.

In Appendix C, full equations of the s@cMBH-disk are derived by simplifying the ecosystem composed of sMBHs inside the cMBH-disk. In the model, sMBHs are dynamically damped so efficiently that they co-rotate with cMBH-disks (Wang et al. 2021a). Motion effects of sMBHs on the Bondi accretion can be neglected. Different points of the s@cMBH-disk system from known models of accretion disks (Shakura & Sunyaev 1973) rest on: 1) extra heating of accretion onto sMBHs ($Q_{\rm AMS}$) beyond accretion of the cMBH; 2) vertical equilibrium jointly governed by the cMBH and the sMBHs; 3) accretion rates of the cMBH

Table 2. Ten representative LRDs

Name	RA	Dec	z	$absorption^b$	$v_{ m abs}^c$	Ref.
Abell 2744-QSO1	3.58	-30.40	7.037	Y	36^{+10}_{-9}	1,2
JADES-28074	189.06	62.27	2.259	N	-	3
RUBIES-EGS-49140	214.89	52.88	6.685	Y	~ 50	4,5
UNCOVER-4286	3.62	-30.42	5.835	N	-	6
6585-58018	150.14	2.34	3.928	N	-	6
$\operatorname{SDSSJ} 1025 + 1402^a$	156.38	14.04	0.101	Y	~ 200	7
CEERS-EGS-1244	215.24	53.03	4.477	N	-	8
RUBIES-UDS-40579	34.24	-5.25	3.113	N	-	6
RUBIES-EGS-42046	214.80	52.79	5.276	Y	~ 160	6,8,9
RUBIES-EGS-55604	214.98	52.96	6.982	Y	-	4

^aLocal analog of LRDs.

decrease with radius due to accretion of sMBHs. For a simple illustration, the total energy budget expressed by Eq. (C21) can be approximated as

$$\sigma_{\rm SB}T_{\rm eff}^4 = Q_{\rm vis} + Q_{\rm AMS},\tag{7}$$

where $Q_{\rm AMS}$ and $Q_{\rm vis}$ are given by Eqs. (C5) and (C20). Notably, the effective temperature distribution of the s@cMBH-disk is changed by $Q_{\rm AMS}$, resulting in a much flatter profiles than $T_{\rm eff} \propto R^{-3/4}$, leading to the rest-frame optical continuum of LRDs (i.e., $F_{\lambda, \rm AMS}$).

Tab. I lists all parameters describing the present model. Defining $Q_{\rm AMS}^0 = \ell_0 L_{\rm Edd}^0 \Sigma_{ullet}^0 (m_{ullet}^0/1 M_{\odot})$ (see Eq. C5), we have only three parameters $(Q_{\rm AMS}^0, \beta_{ullet}, \gamma_{ullet})$ except for accretion rates govern SEDs of the s@cMBH-disk system. In Appendix C.9, we provide structures and emergent SEDs of the s@cMBH-disk for different parameters. As shown there, V-shaped SEDs can be conveniently generated by the s@cMBH-disk system. The SEDs depend mainly on the $(Q_{\rm AMS}^0, \beta_{ullet}, \gamma_{ullet})$ -parameters; in particular, (β, γ) determine the turn-over frequencies of the SEDs.

3.2. sMBH population broadens $H\beta$ line

As embryos of AGNs, the s@cMBH-disk system is of $M_{\bullet} \lesssim \mathcal{M}_{m_{\bullet}}$, where sMBHs play an important role in the vertical structure of the cMBH-disk. Details of the gravity potential of the s@cMBH-disk are very complicated, but we provide a simplified version of the broadening effects of the s@cMBH-disk. The typical FWHM of H β line near the mid-plane is given by FWHM $\approx 2.0 \times 10^3 \left(\mathcal{M}_{m_{\bullet}}/10^8 \, M_{\odot}\right)^{1/2} \, \mathrm{km \ s^{-1}}$ from Eq. (E32) in Appendix E. The popular estimation of the LRDs from Eq. (A1) should be the total masses of the sMBHs and the cMBH, rather than the pure masses of the cMBH. As the LRDs are embryos of AGNs, Eq. (A1) doesn't apply to the estimation of cMBH masses. A recent measurement of a lensed LRD (Juodžbalis et al. 2025a) through dynamics actually still covers the sMBHs. Moreover, the observed Balmer lines are usually fitted by two Gaussian components (e.g. Zhuang et al. 2025; Rinaldi et al. 2024). The broad component is from the normal BLR, and the narrow component originates from the outflowing envelope with characteristic FWHM given by FWHM = $110 \left(\mathcal{M}_{m_{\bullet}}/10^8 M_{\odot}\right)^{1/2} \left(D_{\mathrm{en}}/3 \, \mathrm{pc}\right)^{-1/2} \, \mathrm{km \ s^{-1}}$. Such a component is quite prevalent among the LRDs.

3.3. Absorption features of $H\alpha$ line governed by outflowing clumped-envelopes

During the collapse of primordial clouds, an outflowing envelope is formed by radiation pressure (from AGN or nuclear starbursts; see some historical references) (Matsuda & Satō 1969; Larson 1969; Unno et al. 1967). In Appendix F, we derive the characteristic radius and velocity of the envelope using a simplified model. For the presumed density of the cloud $\rho_{\rm c}=10^{-19}\,{\rm g\,cm^{-3}}$, the derived envelope can explain the observed absorption features of the Balmer lines (which have scarcely been found in normal AGNs). We obtain the characteristic radius of the envelope as $D_{\rm en}\approx 5\,{\rm pc}$, and the velocity of $V_{\rm en}\approx 110\,{\rm km\,s^{-1}}$ from Eqs. (F35) and (F34), respectively. It is composed of clumps with an optical depth of the Balmer absorption as $\tau_{\rm abs}\approx 0.2$ from Eq. (F36). The typical values of the envelope are in good agreement with absorption troughs of the LRDs.

^bAbsorption refers to the absorption signatures of the Balmer lines.

^cVelocity of blueshifted H α absorption component, in units of km s⁻¹.

Ref. 1. Akins et al. (2025); 2. D'Eugenio et al. (2025); 3. Setton et al. (2024);

^{4.} Hviding et al. (2025); 5. Rusakov et al. (2025); 6. Setton et al. (2024);

^{7.} Lin et al. (2025b); 8. Rusakov et al. (2025); 9. Taylor et al. (2025);

3.4. Other properties of LRDs

As shown by Wang et al. (2004), X-rays would be lowered by a factor of 10 in high Eddington ratio AGNs. According to the magnetic field reconnection model of the hot corona, we have shown (Wang et al. 2004) that the fraction of X-rays to the bolometric luminosity decreases with Eddington ratios. Considering this fact, Leung et al. (2024); Lambrides et al. (2024); Inayoshi & Maiolino (2025); Pacucci & Narayan (2024) suggest that the LRDs are undergoing super-Eddington accretion in order to explain their lack of X-rays. The slim disk of the cMBH is radiating the ionizing photons for the broad Balmer lines. Since super-Eddington AGNs usually have smaller amplitudes of variations (Lu et al. 2019), the LRDs should be similar to those local super-Eddington AGNs. Including the cosmological factors, the variability amplitudes will be lowered by a factor of (1+z) showing very weak variations. Considering that the observed UV spectra are jointly contributed by nuclear starburst and s@cMBH-disk in some LRDs, we think that the variations are expected to be difficult to detect in both rest-frame UV and optical bands.

4. APPLICATIONS TO THE LRDS

LRDs show diverse shapes of SEDs. We select several representative LRDs with high signal-to-noise ratios in order to illustrate applications of the present model. The selected LRDs are classified as follows: 1) SEDs obviously need three components (slim disk, s@cMBH-disk and NSBs); 2) SEDs only need two components (slim disk and s@cMBH-disk); 3) multiple NSBs are necessary. Tab. 2 lists the nine LRDs, which not only represent characteristic SED shapes but also across a wide range of redshifts. An analog, SDSS J1025+1402 (Lin et al. 2025c), is also selected.

The fitting scheme is described in Appendix G. We generate $F_{\lambda, {\rm AMS}}$ and $F_{\lambda, {\rm MBH}}$ from the present model and $F_{\lambda, {\rm NSB}}$ continuum through CIGALE (Boquien et al. 2019). Fitting results of three representative LRDs are shown in Fig. 2, 3 and 4, respectively. As a local analog of the LRDs SDSS J1025+1402 (Lin et al. 2025c; Ji et al. 2025b) is classified as the second type shown in Fig. 3. Generally, the s@cMBH-disk model works very well for these LRDs, but we note that the third type needs more stellar components, implying that they underwent multiple starbursts (Kritos & Silk 2025). In a future work, we will develop a more complete model of the stellar components.

5. DISCUSSIONS

There are great efforts to explain LRDs' properties, but most of them only focus on parts of them. On the one hand, these ideas are motivated and highly debated (Juodžbalis et al. 2025b); on the other hand, we should think whether the ingredients of these models can be derived from the simplest hypothesis in order to grasp some of them in a complete model systematically explaining the properties. We list them with brief comments.

5.1. Dust scattering and extinction models

If dust particles scatter the central AGNs, and they are viewed from an edge-on direction, we will see the AGNs as the LRD spectra (Labbe et al. 2025). On the other hand, it has been proposed that LRDs are AGNs but their continuum is highly reddened by dust (Greene et al. 2024; Wang et al. 2024; Kokorev et al. 2024). Both of the models need enough dust particles for LRD properties.

On the observational side, the ALMA observations show that the dust is very dilute (Casey et al. 2024), with even non-detection of dust (Labbe et al. 2025) including both hot and cold dust (Setton et al. 2025), indicating the upper limit of the dust mass is less than $10^6 \, M_\odot$ in 60 LRDs (Casey et al. 2025). Moreover, a stacking analysis of LRD candidates in JADES has shown a distinct lack of hot dust (Eisenstein et al. 2023) (with mean dust masses of $10^4 \, M_\odot$ in LRDs, see Casey et al. 2024, 2025). On the contrary, hot dust generally exists in AGNs ($\gtrsim 10^6 \, M_\odot$ in PG quasars, see Haas et al. 2003). Therefore the LRDs don't have a normal dusty torus in AGNs, and the reddened AGN disk component as the red continuum could be ruled out. Stars in the nuclear regions are so massive through accretion in a dense environment (Wang et al. 2023b) that they directly collapse into sMBHs (Woosley et al. 2002). Here we show that the observed optical continuum is not necessarily reddened by dust, but it is emission from the accretion onto sMBHs in the s@cMBH-disk.

5.2. Gas-enshrouded AGNs

Given the absorption features of the Balmer lines as a common feature, a dense gaseous envelope enshrouding AGNs has been suggested by several authors for the nature of the LRDs (Naidu et al. 2025; Rusakov et al. 2025; Inayoshi & Maiolino 2025) and received much attention. However, this model suffers from the general deficit of IR-weak continuum (de Graaff et al. 2025) as its reprocessing; moreover, the envelope location remains open from 40 AU (Naidu et al. 2025) to 3000 AU (Lin et al. 2025c). In addition, how to form and sustain the envelope remains open.

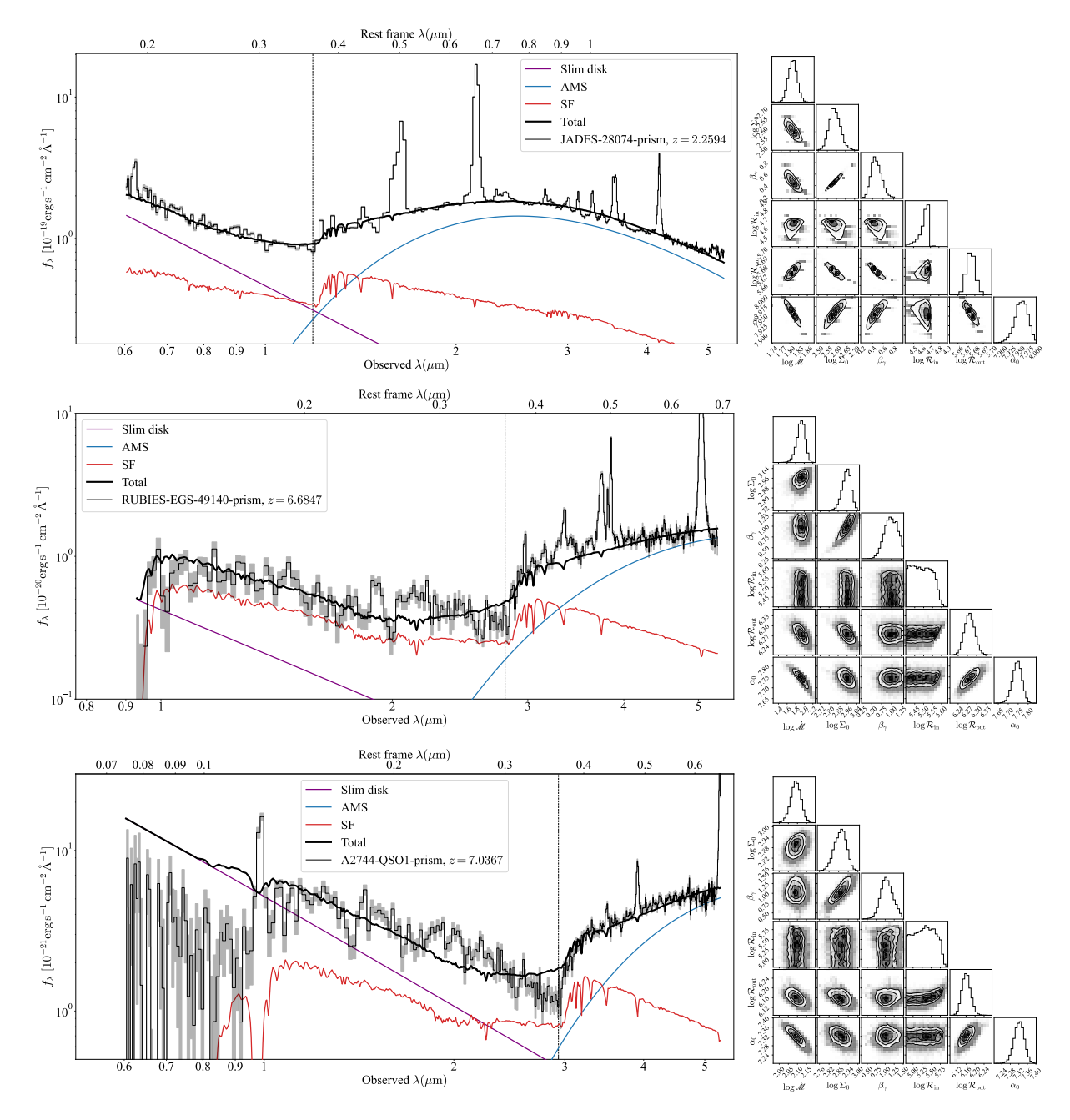


Figure 2. Spectral energy distributions of the represent LRDs with three necessary components. NSB component composes of only single stellar population as the necessary for the part around the Balmer break.

5.3. Thomson broadening effects

Thomson scattering of hot electrons is suggested to efficiently broaden the Balmer lines (Rusakov et al. 2025). After correction of the line width, the cMBH masses are greatly reduced by factors of 10-100. It has been suggested that the electrons could results from winds of super-Eddington accretion (Liu et al. 2025) and could also account for the Balmer break. Narrow-line Seyfert 1 galaxies are known to be super-Eddington accreting AGNs (Du & Wang 2019); however, they have neither the Balmer break nor absorption features of the Balmer lines.

5.4. Starburst

A nuclear pure starburst has been suggested by Baggen et al. (2023). Actually, narrow-line LRDs have been claimed recently (Zhang et al. 2025b), indicating that dusty tori obscure AGNs (this fact conflicts with the non-detection of dust particles by

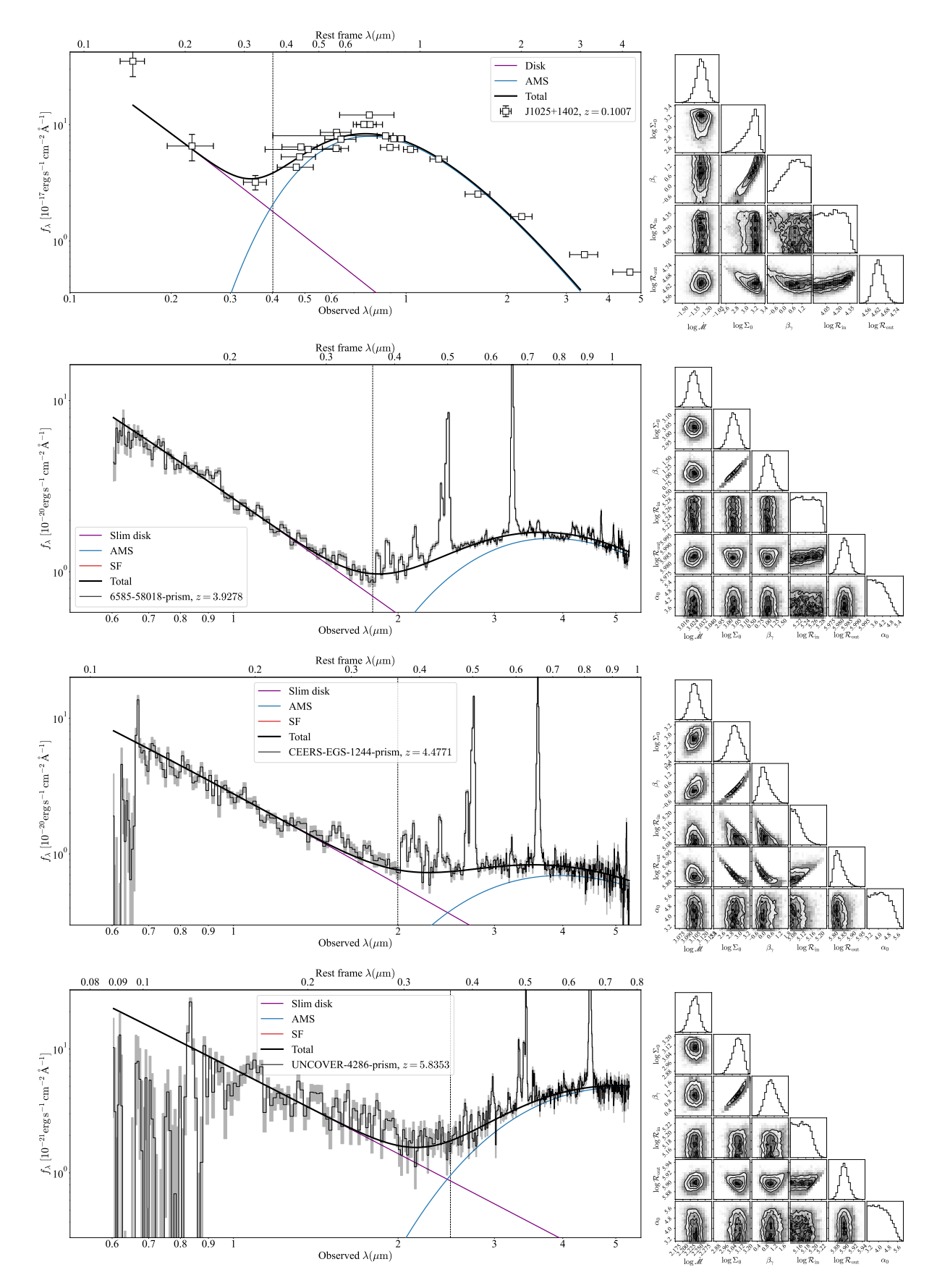


Figure 3. Spectral energy distributions of the represent LRDs with two necessary components contributed by slim disks and s@cMBH-disk. NSB components are not necessary for them.

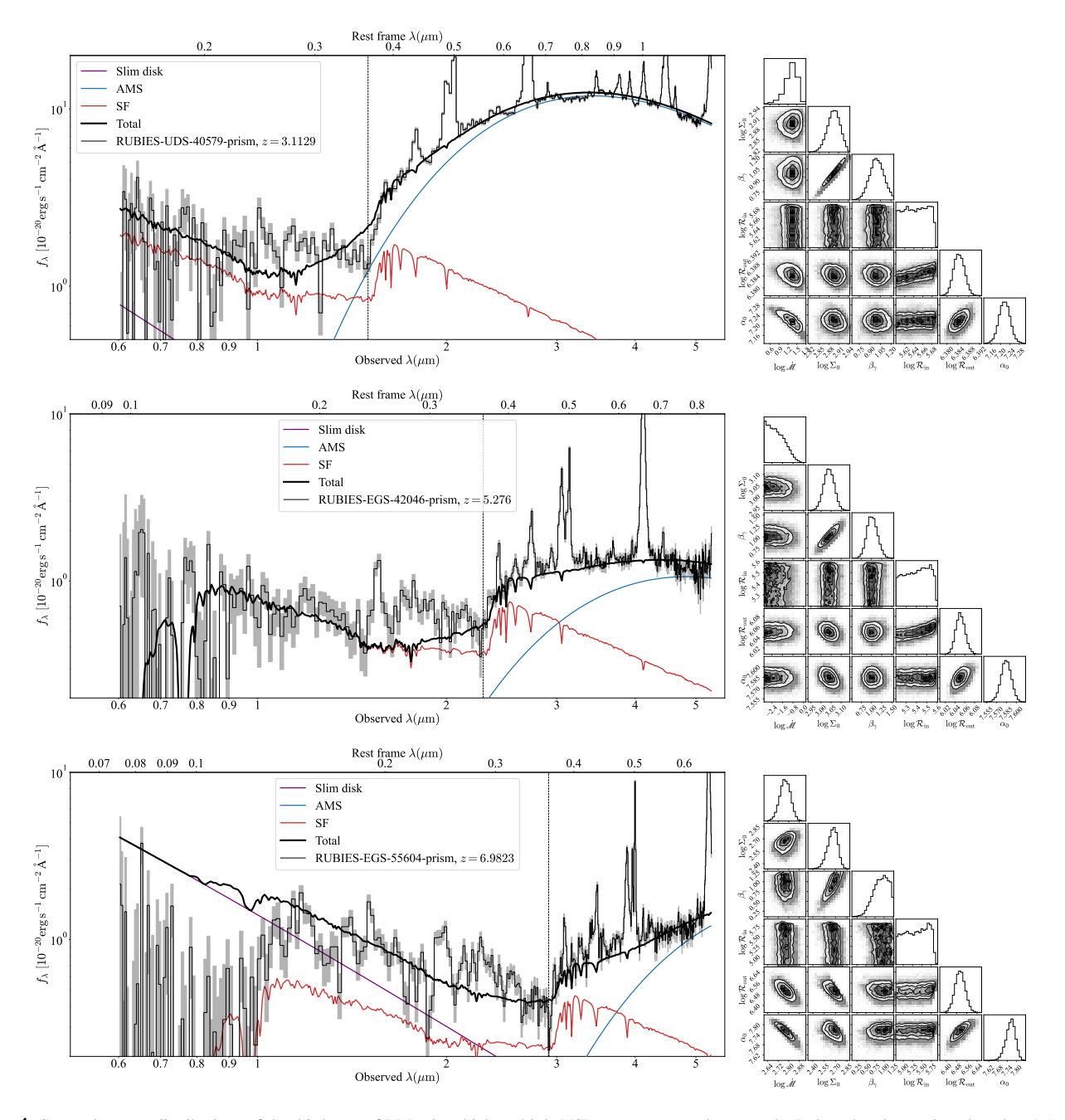


Figure 4. Spectral energy distributions of the third type of LRDs in which multiple NSBs are necessary between the Balmer break wavelength and $\sim 0.2 \,\mu\text{m}$. Sometimes slim disks are not necessary, implying the cMBH masses are quite light (much less than $10^6 \, M_\odot$). We also note that RUBIES-EGS 42046-prisim shows P Cyg profile of the Balmer lines (Hviding et al. 2025).

ALMA observations). However, the observed rest-UV SEDs are different from those of star forming galaxies in the earlier universe (Taylor et al. 2025); meanwhile, they are also different from the standard accretion disk model (known as $F_{\nu} \propto \nu^{1/3}$). The observed rest-UV SEDs could be composed of contributions from s@cMBH-disk and star formation .

5.5. Self-gravitating disk

It has been suggested that the V-shaped SEDs can be formed by a self-gravitating disk corresponding to the Toomer parameter Q=1 (Zhang et al. 2025a; Zwick et al. 2025). However, the observed $\beta_{\rm opt}$ and $\beta_{\rm UV}$ are not related (Zhuang et al. 2025), in disagreement with this model. Moreover, the outer part of accretion disks of normal AGNs and quasars has been known to be

self-gravitating for many years (Sirko & Goodman 2003); however, V-shaped SEDs never appear in these objects. This model generally mismatches the observations.

5.6. *Compactness of the LRDs*

It is a good idea to compare the densities of bulges and nuclear star clusters (NSCs) with the LRDs for their formation and evolution. The mean densities of bulges and NSCs are $\rho_{\rm bulge}^* \sim 25\,M_{11}R_{\rm kpc}^{-3}M_{\odot}\,{\rm pc}^{-3}$ and $\rho_{\rm NSC}^* \sim 2.5\times10^4\,M_8R_{10{\rm pc}}^{-3}M_{\odot}\,{\rm pc}^{-3}$, respectively, where $M_{11}=M_{\rm bulge}/10^{11}M_{\odot}$ and $R_{\rm kpc}=R_{\rm bulge}/1\,{\rm kpc}$ are the bulge stellar masses and radii, respectively; $M_8=M_{\rm NSC}/10^8M_{\odot}$ and $R_{10\,{\rm pc}}=R_{\rm NSC}/10\,{\rm pc}$ are the NSC stellar masses and radii (Neumayer et al. 2020). Baggen et al. (2023) shows that the LRDs have a stellar mass of $\sim 10^9\,M_{\odot}$ with a mean radius of 0.1 kpc, showing a density of $2.5\times10^2\,M_{\odot}\,{\rm pc}^{-3}$. This indicates $\rho_{\rm bulge}^* < \rho_{\rm LRD}^* < \rho_{\rm NSC}^*$, along with the fact that the NSCs follow the $M_{\bullet}-M_{\rm NSC}$ relation in local galaxies (Ferrarese et al. 2006), suggesting that LRDs are still undergoing growth toward quasars and NSCs. Considering the existence of the most luminous LRDs ($L_{5100}\lesssim 2\times10^{44}\,{\rm erg~s^{-1}}$), on the other hand, we may ask what the observational appearance of objects looks like beyond the maximum luminosity of the LRDs in the early universe?

We speculate about their appearance. Usually, the more massive primordial clouds, the higher spin angular momentum from the tidal interaction with their neighbors. The specific SAM is given by $j=\mathcal{J}/M_{\rm c} \propto M_{\rm c}^{2/3}$ (see Eq. (7.172) in Mo et al. 2010). Therefore, there is a critical mass of clouds over which their SAM are not able to remove within local Hubble time by known mechanisms. In such a case, only giant disk galaxies are formed, but the cMBHs are tiny (even without cMBHs).

5.7. Heuristic ideas

Three major properties at least should be grasped in a successful model: 1) avoiding the Soltan crisis; 2) a natural mechanism for an outflowing envelope is necessary for absorption features of the Balmer lines; 3) the rest-frame optical continuum as a bump without dust extinction. These necessary elements motivate us to propose the current model composed of three ingredients formed during the collapsing periods of the primordial clouds:

$$\boxed{LRDs} = \boxed{\text{outflowing envelope}} \oplus \boxed{\text{s@cMBH-disk system}} \oplus \boxed{\text{nuclear starburst}}$$

Cartoon in Fig. 1 shows the structure. While nuclear starbursts form from a rapid collapse of the clouds (Vanzella et al. 2019), the outflowing envelope is driven by the starburst or AGN activity. With sufficient angular momentum of the nuclear regions, s@cMBH-disk is formed. We would point out that the starburst could have extreme top-heavy mode so that massive stars directly collapse into sMBHs without explosion (Woosley et al. 2002) yielding much fewer metal elements for dust particles in the nuclear regions.

6. CONCLUSIONS

We demonstrate that the cMBHs in LRDs can not exceed $10^6 M_{\odot}$ in light of the Soltan argument of the current data. A population of sMBHs embedded inside the accretion disks of the cMBH is responsible for the rest-frame optical continuum. This constitutes the embryo structure of AGNs and reveals the nature of LRDs. The sMBHs are the remnants of stellar evolution as a natural consequence of the cMBH formation through the gravitational collapse of primordial clouds. The cMBH-disk, or jointly with the post starburst, powers the UV continuum. The observed V-shaped SEDs of LRDs can be well explained by the s@cMBH-disk scenario. Meanwhile, the radiation pressure drives the collapsing cloud to form an envelope generating the observed absorption features of the Balmer lines. Other properties of the LRDs, such as non-variable continuum and lack of X-ray emission, can be explained by the present model.

Internal and external factors govern the evolution of the LRDs on different timescales. First, internal mechanisms drive mergers and inward migrations of sMBHs in the cMBH-disk (Tagawa et al. 2020; Wang et al. 2021b; Vaccaro et al. 2025), whose gravitational waves could be detected by the future LISA (Amaro-Seoane et al. 2023)/Tianqin (Luo et al. 2025) and the Einstein Telescope (Di Giovanni 2025), even by the current LIGO, providing conclusive tests of the s@cMBH-disk model for LRDs. Meanwhile, this leads to evolutionary decays and shifts of the V-shaped SEDs, and the Balmer absorption features since the envelope is gradually blow away, appearing either as narrow-line Seyfert 1 galaxies, or as compact galaxies. Successive hierarchical mergers finally yield a small number of cMBHs in the centers. Moreover, the volume densities of LRDs are so high that their merger rates are very frequent, leading to the formation of new LRDs or galaxies (Billand et al. 2025).

- This research is supported by NSFC-12333003, -92476203, -12521005, -12573016, the National Key R&D Program of
- ² China (2021YFA1600404, 2023YFA1607903, and 2023YFA1607904), the National Science and Technology Major Project
- (2024ZD0300303), the China Manned Space Project (CMS-CSST-2025-A07), and the Strategic Priority Research Program of
- the Chinese Academy of Sciences (XDB1160202).

APPENDIX

A. CONVENTIONAL ESTIMATIONS OF THE CMBH

Though the LRDs are poorly understood, astronomers have to estimate the cMBH masses in light of the so-called R-L relation established for AGNs (Maiolino et al. 2024a) though there are growing serious challenges to this relation (Du & Wang 2019; Wang et al. 2025a). The currently popular estimations of their cMBH masses follow that for normal AGNs through H α or H β lines (Greene & Ho 2005)

$$M_{\bullet} = (2.0, 3.6) \times 10^{6} \left(\frac{L_{\text{H}\alpha, \text{H}\beta}}{10^{42} \text{erg s}^{-1}} \right)^{0.56} \left[\frac{\text{FWHM}(\text{H}\alpha, \text{H}\beta)}{10^{3} \text{ km s}^{-1}} \right]^{2.06} M_{\odot}, \tag{A1}$$

respectively. We should emphasize here that Eq. (A1) is based on the original R-L relation (Kaspi et al. 2000; Bentz et al. 2013; Du & Wang 2019) and an assumption that there is a single cMBH surrounded by virialized motions of BLR clouds, in particular, this estimation only applies to sub-Eddington accreting AGNs (Du & Wang 2019).

In the proposed model, the cMBH mass is smaller than the total masses of sMBHs embedded in the s@cMBH-disk. Estimations of total sMBH masses become quite complicated, but we show it in Appendix E. According to Eq. (A1), the LRDs have overmassive cMBHs compared with the Magorrian relation (Magorrian et al. 1998). Recently, a direct measurement of one LRD shows evidence for an SMBH ($\sim 10^8~M_{\odot}$) in Abell 2744-QSO1 (Juodžbalis et al. 2025a), but within a region of 20-150~pc. The proposed population of sMBHs may exist within the above region, and their measurements should cover the sMBHs. The mean cMBH masses should be smaller than that given by Eq. (A1) avoiding the crisis of the Soltan argument (Soltan 1982; Chokshi & Turner 1992; Yu & Tremaine 2002; Jahnke 2025) briefly discussed below.

B. INNER STRUCTURES OF PHL 1092

Reverberation mapping of AGNs is a powerful tool probing their inner structures (Blandford & McKee 1982). Since the 1980s, RM of about 300 AGNs has been done for H β delays, but targets of long-term campaigns (longer than 6-7 years) with high cadences are quite limited (see a brief summary in Wang et al. 2025a). There is growing evidence for anomalous reverberations of the broad H β line with respect to the varying continuum (Wang et al. 2025a). It has been found that the delays of the H β line decrease with accretion rates (Du et al. 2014; Wang et al. 2014; Du & Wang 2019); in particular, the quasar PHL 1092 shows leading reverberations of H β line (Wang et al. 2025a) in advance of 17 – 57 days relative to the varying 5100 Å continuum. These extreme reverberations suggest that there are extra energy sources which spatially distribute over the accretion disks of the cMBH. This phenomenon offers a new perspective for understanding the internal structure of AGNs.

A population of sMBHs has been suggested to be the extra energy sources (Wang et al. 2025a), which efficiently heat the cMBH-disk. SEDs emerging from such a disk depend on two key parameters (see Appendix C): spatial distributions of sMBHs and their mass functions. For the LRDs, they are located in outskirts of the disks and thus gravitational energy is mainly released in optical bands. On the other hand, migration of sMBHs towards the cMBH makes the rest-frame optical continuum shift to UV bands. Therefore, SEDs indicate the evolutionary stage of migration of the sMBH population from embryos to normal AGNs.

C. STRUCTURES AND SEDS OF THE s@cMBH-disk

C.1. Evidence for sMBHs in AGNs

Compact objects embedded inside accretion disks of SMBHs in AGNs have been considered by (Cheng & Wang 1999), and later by (McKernan et al. 2011; Tagawa et al. 2020; Vaccaro et al. 2025). LIGO may have already detected such an event (GW 190521) (Graham et al. 2020), and more candidates (Graham et al. 2023), in particular, a merger of $137^{+22}_{-17} M_{\odot}$ and $103^{+20}_{-52} M_{\odot}$ was detected recently (The LIGO Scientific Collaboration et al. 2025). Owing to its powerful spatial resolution, GRAVITY on Very Large Telescopes Interferometer (VLTI) of European Southern Observatory (ESO) depicts accurately enough the positions of flares of Sgr A* and find that they are distributed over a ring with $\sim 9R_{\rm g}$. Such flares cannot be generated by magnetic reconnection randomly happening on the disk surface, but could be produced by an orbiting $\sim 40 M_{\odot}$ black hole around the cMBH (Wang et al. 2023a). Additionally, there is growing evidence for the presence of satellite black holes around the cMBH from X-ray observations. In AGN 1ES 1927+654, mHz quasi-periodic oscillations (QPOs) of X-ray variations (Masterson et al. 2025), and in GSN 069 as a Seyfert 2 galaxy, quasi-periodic ejections (QPEs) (Miniutti et al. 2019) and others (Giustini et al. 2020; Arcodia et al. 2021; Chakraborty et al. 2021; Arcodia et al. 2024), significantly enhance the validity of sMBH in AGN disk. This also lends support to the proposition that LRDs contain a population of sMBHs in the cMBH-disk.

C.2. Accretion onto sMBH and radiation

Considering that the s@cMBH-disk contains a population of sMBHs, we have to reconsider the basic equations of accretion disks (Kato et al. 1998; Frank et al. 2002) of the s@cMBH-disk since there is additional heating of sMBHs and decreases of \dot{M}_{\bullet} along with R due to accretion onto sMBHs. Gilbaum & Stone (2022); Zhou et al. (2024); Wang et al. (2025a) have studied the equations of s@cMBH-disk, but we revisit all the equations of s@cMBH-disk by including more realistic and necessary considerations. We first consider the heating of sMBHs.

The ideal Bondi accretion rates are extremely super-Eddington though the heating and viscosity effects efficiently reduce them (Luo & Wang 2025). For super-Eddington accretion onto sMBHs, the radiated luminosity could be saturated at a few times the Eddington luminosity with a factor of logarithmic dependence of accretion rates (Abramowicz et al. 1988; Wang & Zhou 1999; Mineshige et al. 2000; Yoshioka et al. 2024). On the other hand, we note that outflows are developed from the slim accretion disks, but the mechanical power is always less than the saturated (Yoshioka et al. 2024). Nevertheless, it is interesting to note that most gas is circulated by the outflows, roughly remaining the gas of the cMBH-disk there. Keeping these uncertainties of energies released by sMBH accretion in mind, we approximately take a simple radiative luminosity from the accretion onto sMBHs as

$$\ell_{\bullet} = \ell_0 L_{\rm Edd}^0 \left(\frac{m_{\bullet}}{1 \, M_{\odot}} \right), \tag{C2}$$

where ℓ_0 is the factor of the saturated luminosity and could be in a range of $\ell_0 \approx 1 \sim 10$, $L_{\rm Edd}^0 = 1.4 \times 10^{38} \, {\rm erg \ s^{-1}}$ is the Eddington luminosity of $1 \, M_{\odot}$ black hole. In our previous paper (Zhou et al. 2024), we simply take the Eddington luminosity as their radiative luminosity independent of density and temperature. We assume that the energy from AMSs are thermalized locally.

The mass function of sMBHs is important but it depends on their accretion. Considering that the sMBHs are growing with migration inward, we neglect the complicated details of their growth and presume a formulation of

$$m_{\bullet}(R) = m_{\bullet}^{0} \left(\frac{R}{\mathcal{R}_{\text{out}}}\right)^{\beta_{\bullet}},$$
 (C3)

where m_{\bullet}^0 is the sMBH mass at radius \mathcal{R}_{out} . Assuming that the surface number density of sMBHs is

$$\Sigma_{\bullet} = \Sigma_{\bullet}^{0} \left(\frac{R}{\mathcal{R}_{\text{out}}}\right)^{\gamma_{\bullet}},\tag{C4}$$

with $\gamma_{\bullet} > 0$ (the surface number density decreases inward due to mergers), we have the heating rate of the accreting sMBHs per unit area

$$Q_{\rm AMS} = \ell_0 \Sigma_{\bullet}^0 \left(\frac{m_{\bullet}^0}{1 \, M_{\odot}} \right) \left(\frac{R}{\mathcal{R}_{\rm out}} \right)^{\beta_{\bullet} + \gamma_{\bullet}} = Q_{\rm AMS}^0 \left(\frac{R}{\mathcal{R}_{\rm out}} \right)^{\beta_{\bullet} + \gamma_{\bullet}}, \tag{C5}$$

where $Q_{\rm AMS}^0 = \ell_0 L_{\rm Edd}^0 \Sigma_{ullet}^0 \left(m_{ullet}^0 / 1 \, M_{\odot} \right)$ is a constant parameter. The total numbers and masses of sMBHs are given by

$$\mathcal{N}_{\bullet} = 2\pi \int_{\mathcal{R}_{\text{in}}}^{\mathcal{R}_{\text{out}}} \Sigma_{\bullet} R dR = \frac{2\pi \mathcal{R}_{\text{out}}^2 \Sigma_{\bullet}^0}{2 + \gamma_{\bullet}} \left[1 - \left(\frac{\mathcal{R}_{\text{in}}}{\mathcal{R}_{\text{out}}} \right)^{2 + \gamma_{\bullet}} \right], \tag{C6}$$

and

$$\mathcal{M}_{m_{\bullet}} = 2\pi \int_{\mathcal{R}_{\text{in}}}^{\mathcal{R}_{\text{out}}} \Sigma_{\bullet} m_{\bullet} R dR = \frac{\mathcal{M}_{m_{\bullet}}^{0}}{1 + \beta_{\gamma}} \left[1 - \left(\frac{\mathcal{R}_{\text{in}}}{\mathcal{R}_{\text{out}}} \right)^{1 + \beta_{\gamma}} \right], \tag{C7}$$

where $\mathscr{M}_{m_{\bullet}}^{0}=2\pi\mathcal{R}_{\mathrm{out}}^{2}\Sigma_{\bullet}^{0}m_{\bullet}^{0}$, $\beta_{\gamma}=1+\beta_{\bullet}+\gamma_{\bullet}$. For typical values obtained from fittings of the 10 representative LRDs in Appendix G, we have $\mathscr{N}_{\bullet}\sim10^{6}$, $\mathscr{M}_{m_{\bullet}}\sim10^{6}\,M_{\odot}$ in light of $\mathcal{R}_{\mathrm{out}}\sim20\,\mathrm{ltd}$, $\mathcal{R}_{\mathrm{in}}\sim1\,\mathrm{ltd}$, and $\beta_{\gamma}\sim0.8$.

C.3. Mass conservation

First of all, accretion rates of the s@cMBH-disk are a function of radius due to accretion on sMBHs. The mass conservation equation reads

$$\dot{M}_{\bullet}(R) = -2\pi R V_{\rm R} \Sigma_{\rm gas},\tag{C8}$$

where $V_{\rm R}$ is the radial velocity of accreted gas, $\Sigma_{\rm gas} = 2\rho H$ is the surface density of the disk and ρ is the gas density. Given the heating rates per unit area due to sMBHs, red the mass accretion rate onto sMBHs in a ring of width ${\rm d}R$ is $2\pi RQ_{\rm AMS}{\rm d}R/\eta_{\bullet}c^2$, which is equal to the decrease in the accretion rate of the s@cMBH-disk. We have

$$\frac{\mathrm{d}\dot{M}_{\bullet}}{\mathrm{d}R} = 2\pi\eta_{\bullet}^{-1}c^{-2}RQ_{\mathrm{AMS}},\tag{C9}$$

yielding

$$\dot{M}_{\bullet} = \dot{M}_{\bullet}^{0} - \frac{2\pi Q_{\rm AMS}^{0} \mathcal{R}_{\rm out}^{2}}{(1 + \beta_{\gamma})\eta_{\bullet}c^{2}} \left[1 - \left(\frac{R}{\mathcal{R}_{\rm out}}\right)^{1 + \beta_{\gamma}} \right], \tag{C10}$$

where \dot{M}_{\bullet}^0 is the rates at $\mathcal{R}_{\mathrm{out}}$. \dot{M}_{\bullet} decreases inward with decreasing R. Considering that most of the accreted gas will be channeled into outflows (Yoshioka et al. 2024), here we assume $\eta_{\bullet} \approx 0.1$ for a simple treatment. Eqs. (C8) and (C10) lead to V_R after determining Σ_{gas} . This effect has not been included by Gilbaum & Stone (2022); Zhou et al. (2024); Xu et al. (2025). As a simplified treatment, this estimation accounts for the returned gas from outflow of accretion onto sMBHs by neglecting the details.

C.4. Vertical equilibrium

We assume that the vertical structure of the s@cMBH-disk system is in static equilibrium, but the vertical gravity force $(F_{m_{\bullet}}^z)$ of the sMBHs should be included

$$\frac{1}{\rho} \left(\frac{\mathrm{d}P}{\mathrm{d}z} \right) = \frac{GM_{\bullet}}{R^2} \left(\frac{H}{R} \right) + F_{m_{\bullet}}^z, \tag{C11}$$

The details of the $F_{m_{\bullet}}^z$ are quite complicated, but we adopt the approximation $F_{m_{\bullet}}^z \approx 2\pi f_0 G \Sigma_{\bullet}$, which is from an infinite plane with homogeneous surface mass density, where $f_0 \approx 0.9$ is a correction factor of the force. We note that this approximation is valid for $H/R \lesssim 0.1$ within about 10% accuracy in light of the detailed calculations (Huré & Hersant 2011) . Following the common approximate treatment of the vertical structure, we re-cast Eq. (C11)

$$\frac{1}{\rho} \left(\frac{P}{H} \right) = \frac{GM_{\bullet}}{R^2} \left(\frac{H}{R} \right) + 2\pi f_0 G \Sigma_{\bullet}. \tag{C12}$$

It is clear that $F_{m_{\bullet}}^{z}$ stabilizes the vertical structure.

In order to obtain the energy releasing rates of the s@cMBH-disk and gravity-broadening effects, we have to solve the Poisson equation of $\nabla \phi = 4\pi \rho_{\bullet}(r,z)$ for the s@cMBH-disk potential. One analytical approximate solution with an accuracy of 10% has been derived (Huré & Hersant 2011),

$$\phi(R) \approx -\frac{G\mathcal{M}_{m_{\bullet}}^{0}}{\mathcal{R}_{\text{out}}} \left\{ \frac{1}{\beta_{\gamma}} + \left[0.431 - \frac{1}{\beta_{\gamma}(1+\beta_{\gamma})} \right] \left(\frac{R}{\mathcal{R}_{\text{out}}} \right)^{\beta_{\gamma}} - \frac{1}{1+\beta_{\gamma}} \left(\frac{\mathcal{R}_{\text{in}}}{\mathcal{R}_{\text{out}}} \right)^{\beta_{\gamma}} \frac{\mathcal{R}_{\text{in}}}{R} \right\} - \frac{GM_{\bullet}}{R}, \quad (C13)$$

yielding angular velocity

$$\Omega_{K} = \left(\frac{1}{R} \frac{d\phi}{dR}\right)^{1/2} = \sqrt{\frac{G\mathcal{M}_{m_{\bullet}}^{0}}{\mathcal{R}_{out}}} \frac{\mathscr{F}_{R}}{R^{2}} + \frac{GM_{\bullet}}{R^{3}},\tag{C14}$$

where

$$\mathscr{F}_{R} = \left[\frac{1}{1 + \beta_{\gamma}} - 0.431 \beta_{\gamma} \right] \left(\frac{R}{\mathcal{R}_{\text{out}}} \right)^{\beta_{\gamma}} - \frac{1}{1 + \beta_{\gamma}} \left(\frac{\mathcal{R}_{\text{in}}}{\mathcal{R}_{\text{out}}} \right)^{\beta_{\gamma}} \frac{\mathcal{R}_{\text{in}}}{R}.$$
 (C15)

The roles of sMBHs in the vertical equilibrium have not been considered in Gilbaum & Stone (2022) and Zhou et al. (2024).

C.5. Conservation of angular momentum

The conservation equation of angular momentum reads

$$R\frac{\partial(\Sigma_{\text{gas}}R^2\Omega_{\text{K}})}{\partial t} + \frac{\partial}{\partial R}\left(R\Sigma_{\text{gas}}V_RR^2\Omega_{\text{K}}\right) = \frac{1}{2\pi}\frac{\partial\mathcal{G}}{\partial R},\tag{C16}$$

where \mathcal{G} is the viscosity stress. For a stationary state, by using Eq. (C8), we have

$$-\frac{\partial}{\partial R} \left(\frac{\dot{M}_{\bullet}}{2\pi} R^2 \Omega_{\rm K} \right) = \frac{\partial}{\partial R} \left(R^3 \nu \Sigma_{\rm gas} \frac{\mathrm{d}\Omega_{\rm K}}{\mathrm{d}R} \right). \tag{C17}$$

Similar to the standard model of accretion disk, we use the torque-free boundary condition at the inner edge of the s@cMBH-disk part, i.e., the region between \mathcal{R}_{in} and \mathcal{R}_{out} , and we have

$$\frac{1}{2\pi} \left[R^2 \Omega_{K}(R) \dot{M}_{\bullet}(R) - \mathcal{R}_{in}^2 \Omega_{K}(\mathcal{R}_{in}) \dot{M}_{\bullet}(\mathcal{R}_{in}) \right] = -R^3 \nu \Sigma_{gas} \left(\frac{d\Omega_{K}}{dR} \right). \tag{C18}$$

after integrating Eq. (C17). This boundary condition holds approximately for LRDs since sMBHs are located at the disk outskirts. Defining $\ell=R^2\Omega_{\rm K}(R)$ and $\ell_{\rm in}=\mathcal{R}_{\rm in}^2\Omega_{\rm K}(\mathcal{R}_{\rm in})$, we have

$$\nu \Sigma_{\rm gas} = \frac{\dot{M}_{\bullet}}{2\pi} \left[\frac{\dot{M}_{\bullet}(\mathcal{R}_{\rm in})\ell_{\rm in}}{\dot{M}_{\bullet}\ell} - 1 \right] \left(\frac{\mathrm{d}\ln\Omega_{\rm K}}{\mathrm{d}\ln R} \right)^{-1}. \tag{C19}$$

C.6. Energy balance

The viscous heating rate per unit area can be expressed by

$$Q_{\text{vis}} = \int_{-H}^{H} \nu \rho \left(R \frac{d\Omega_{\text{K}}}{dR} \right)^{2} dz = \nu \Sigma_{\text{gas}} \left(R \frac{d\Omega_{\text{K}}}{dR} \right)^{2} = T_{r\varphi} R \frac{d\Omega_{\text{K}}}{dR}, \tag{C20}$$

where $T_{r\varphi} = \nu \Sigma R d\Omega_K / dR$. Using Eq. (C5), we have the energy equation $Q_+ = Q_{vis} + Q_{AMS}$

$$Q_{+} = Q_{\text{rad}},\tag{C21}$$

and the surface cooling rates are given by

$$Q_{\rm rad} = \frac{2\sigma_{\rm SB}T^4}{\tau_{\rm eff}}, \quad \tau_{\rm eff} = \frac{3\tau}{8} + \frac{1}{2} + \frac{1}{4\tau}, \quad T_{\rm eff} = \tau_{\rm eff}^{-1/4}T$$
 (C22)

where T is the temperature of the mid-plane of the accretion disk, $T_{\rm eff}$ is the effective temperature, and the optical depth of the s@cMBH-disk is $\tau = \kappa_R \rho H$. We would point out that the first term on the right-hand side of Eq. (C21) covers the energy released by cMBH-disk, including the potential of sMBHs; whereas it is not included in (Gilbaum & Stone 2022).

C.7. Viscosity and state equation

The $r\varphi$ -component of the shearing stress tensor can be expressed by

$$t_{r\varphi} = \rho \nu R \frac{\mathrm{d}\Omega_{K}}{\mathrm{d}R} = \rho \nu \Omega_{K} \frac{\mathrm{d}\ln\Omega_{K}}{\mathrm{d}\ln R} = -\alpha P. \tag{C23}$$

The speed of sound is $c_{\rm s}=\sqrt{\gamma P/\rho}$, where γ is gas index, P is the total pressure, and ρ is the disk density at the mid-plane. With inclusion of the radiation pressure, we have the total pressure

$$P = \frac{k_{\rm B}}{\mu m_{\rm p}} \rho T + \frac{\tau \sigma_{\rm SB}}{2c} T_{\rm eff}^4, \tag{C24}$$

where $k_{\rm B}$ is the Boltzmann constant, $m_{\rm p}$ is the proton mass, and μ is the mean molecular mass. All these equations above formed a closed system for parameters ρ , T, H and V_R .

C.8. Total gas mass of the s@cMBH-disk

The total gas mass of the s@cMBH-disk is then given by

$$\mathcal{M}_{\text{gas}} = 2\pi \int_{\mathcal{R}_{\text{in}}}^{\mathcal{R}_{\text{out}}} \Sigma_{\text{gas}} R dR = 1.4 \times 10^3 \, M_{\odot}, \tag{C25}$$

for $\dot{\mathcal{M}}=10^2$ at $R_{\rm out}$, $(\mathcal{R}_{\rm in},\mathcal{R}_{\rm out})=\left(10^5,10^6\right)\,R_{\rm g}\,(R_{\rm g}=1.5\times10^{10}\,M_{\rm 5}\,{\rm cm}$ and $M_5=M_{\bullet}/10^5\,M_{\odot}$), and $\beta_{\gamma}=1$. External supply of gas outside the s@cMBH-disk is necessary to maintain the disk.

As a summary, Eqs. (C8, C10, C12, C19, C21, C24) describe the structure and radiation of the s@cMBH-disk and their solutions provide results.

C.9. Emergent spectra from the s@cMBH-disk

We examine the temperature of the s@cMBH-disk through the blackbody approximation obtained by

$$T = \left(\frac{L_{\text{Bol}}}{\pi \sigma_{\text{SB}} R_{\text{disk}}^2}\right)^{1/4} \approx 3.8 \times 10^3 L_{44}^{1/4} R_{\text{disk},20}^{-1/2} \,\text{K},\tag{C26}$$

where $\sigma_{\rm SB} = 5.67 \times 10^{-5}$ is the Stefan-Boltzmann constant, $L_{44} = L_{\rm Bol}/10^{44}\,{\rm erg~s^{-1}}$ is the total bolometric luminosity of the sMBH accretion, and $R_{\rm disk,20} = R_{\rm disk}/20\,{\rm ltd}$ is the typical radius of the s@cMBH-disk (overlapping with the BLR). In such a circumstance of $T \sim 3800\,{\rm K}$, bound-bound, bound-free and free-free absorptions are important, and SEDs from this part of the disk will mainly contribute to optical bands as the origin of the V-shaped SEDs of LRDs.

The emergent spectra rely on self-consistent calculations of vertical structure of the s@cMBH-disk, such as done for the case based on standard model of the Shakura-Sunyaev disk (Ross et al. 1992; Shimura & Takahara 1993; Wang et al. 2025b). However, this paper concentrates on the characteristic spectra of the s@cMBH-disk by taking the simple analytic approach of the vertical structure (Hubeny 1990). Combining Eqs. (C19), (C21), (C22), we can have the effective temperature distributions for the emergent spectra without knowing the structure of the s@cMBH-disk unless the s@cMBH-disk is optically thick. This is similar to the standard model of accretion disk because we assume the Keplerian rotation here. The total emissions from the s@cMBH-disk can be obtained by

$$F_{\lambda,\text{AMS}} = \frac{2\pi \cos i}{D_{\text{L}}^2} \int_{\mathcal{R}_{\text{in}}}^{\mathcal{R}_{\text{out}}} B_{\lambda}(T_{\text{eff}}) R dR, \tag{C27}$$

over the s@cMBH-disk, i is the inclinations and D_L is the luminosity distance of a LRD.

In principle, the gas self-gravity of the s@cMBH-disk could be important (Sirko & Goodman 2003; Zhang et al. 2025a) but the accreting sMBHs dominate the heating of the self-gravity. We show that such an sMBH disk with gas is stable in Appendix C. We neglect the effects of gravity in this paper. In this paper, we take $r_{\rm in} = 6R_{\rm g}$ (for a non-spinning cMBH) and $\mathcal{R}_{\rm in} = r_{\rm out}$ as a free parameter bridging the two parts of the s@cMBH-disk. On the other hand, $\mathcal{R}_{\rm in}$ and $r_{\rm out}$ could be independent but they depend on $\dot{\mathcal{M}}$ and sMBH spatial distributions and mass functions.

C.10. Slim part of the cMBH-disks

The cMBH has its own disk with outer radius $\mathcal{R}_{\rm out}=R_{\rm in}$. The slim disk equations are taken from Abramowicz et al. (1988) and Mineshige et al. (2000). The vertical equilibrium is given by $H=c_{\rm s}/\Omega_{\rm K}$ and the mass conservation yields $\dot{M}_{\bullet}=4\pi R H \rho V_{\rm R}$, where $V_{\rm R}$ is the radial velocity of the accretion flow. The radial motion is given by

$$\frac{1}{\rho} \frac{\mathrm{d}P}{\mathrm{d}R} - \left(\Omega^2 - \Omega_{\mathrm{K}}^2\right) R + V_{\mathrm{R}} \frac{\mathrm{d}V_{\mathrm{R}}}{\mathrm{d}R} = 0, \tag{C28}$$

and angular momentum

$$\dot{M}_{\bullet}(\ell - \ell_{\rm in}) = 4\pi R^2 H \alpha P,\tag{C29}$$

where ℓ and $\ell_{\rm in}$ are specific angular momentum at R and $r_{\rm in}$ of the slim disk. Here α is the α -description of the viscosity. The energy equation reads

$$\dot{M}_{\bullet}(\ell - \ell_{\rm in}) \left(-\frac{\mathrm{d}\Omega}{\mathrm{d}R} \right) + \dot{M}_{\bullet}T \left(\frac{\mathrm{d}S}{\mathrm{d}R} \right) = 4\pi R F_{\rm rad},$$
 (C30)

where the entropy and surface cooling rates are given by

$$TdS = \frac{P}{\rho} \left[\left(12 - \frac{21}{2} \beta_{\rm d} \right) \frac{dT}{T} - \left(4 - \beta_{\rm d} \right) \frac{d\rho}{\rho} \right], \quad F_{\rm rad} = \frac{c}{\kappa \rho} \frac{aT^4}{3H}, \tag{C31}$$

respectively. Here $\beta_{\rm d}=P_{\rm gas}/\left(P_{\rm gas}+P_{\rm rad}\right)$ is the fraction of gas pressure to the total, $P_{\rm rad}=aT^4/3$ is the radiation pressure in the slim disk, κ is the opacity of the disk. Replacing F_{λ} with $B_{\lambda}(T)$ in Eq. (C27), we get the continuum, where B_{λ} is the Planck function. The slim disks approach the standard accretion disks when $\dot{\mathcal{M}}$ is small enough.

We would point out the issue of the connection between the s@cMBH-disk and the slim disk. At large radii, the slim disk reduces to the standard disk, but it will mismatch the s@cMBH-disk solution because we artificially shut off the AMS heating at $\mathcal{R}_{\rm in}$. It is therefore expected that the discontinuity in density and temperature exists between the slim disk and the s@cMBH-disk, but we take the accretion rates to be continuous. This discontinuity doesn't affect SEDs significantly since little energy is released in this region.

D. PROPERTIES OF cMBH-DISK

Since accretion rates decrease with radius as shown by Eq. (C10), we give \dot{M}_{\bullet}^0 at $\mathcal{R}_{\rm out}$ as the accretion rate at the outer boundary of the s@cMBH-disk. There is a critical value of \dot{M}_{\bullet}^0 , with which $\dot{M}_{\bullet}=0$ at $\mathcal{R}_{\rm in}$ according to Eq. (C10). In this paper, we focus on the case in which \dot{M}_{\bullet}^0 is large enough so that \dot{M}_{\bullet} doesn't vanish at $\mathcal{R}_{\rm in}$. Though there are ten parameters, the structures and SEDs mainly rely on three parameters ($\mathcal{M}_{m_{\bullet}}$, β_{γ} and \dot{M}_{\bullet}^0). Structures of the s@cMBH-disk for different values of the parameters are shown in Fig. 5.

For a fixed $M_{\bullet} = 10^5 \, M_{\odot}$, the structure's dependence on $\mathcal{M}_{m_{\bullet}}$ shows interesting properties on the AMS heating. First, the disk densities and temperatures sensitively increase with $\mathcal{M}_{m_{\bullet}}$ whereas H/R decreases with $\mathcal{M}_{m_{\bullet}}$. AMS heating increases the temperature, and the vertical gravity of AMSs compresses the disk height, leading to increases of disk densities. Second, disk densities, temperatures, optical depth and height monotonically increase with \mathcal{M} . All these properties are easily understood. Third, the structure properties are quite sensitive to β_{γ} . Since the mass function and spatial distributions are degenerate in the heating functions (Eq. C5), we are not able to separate them. The third line panels show the dependence on β_{γ} , in particular, the temperatures and optical depth on β_{γ} as well as SEDs. More steeper β_{γ} more inner structures will be modified.

Fig. 6 shows SED dependence on the parameters. The slim disk of the cMBH contributes to the UV continuum while the s@cMBH-disk provides the optical continuum. Generally, the total SEDs show V-shapes and the turnover frequencies depend on the relative contributions of the slim disks and the s@cMBH-disk. The total SEDs mainly depend on $\mathcal{M}_{m_{\bullet}}$, $\dot{\mathcal{M}}$ and β_{γ} . In particular, β_{γ} affects the SED shapes of s@cMBH-disk, as shown by the fourth row and left panel. This is caused by the facts that energy densities of the s@cMBH-disk contributions increase with steeper β_{γ} increasing the temperatures of the s@cMBH-disk.

E. PROFILES OF BROAD H β LINE

The observed broad H β line is generated by the gravity of the s@cMBH-disk system. In this section, we calculate the profile of broad H β line for a given spatial distribution of sMBHs. The rotation velocity is given by $V_c(R) \approx \Omega_K R$, and leads to width of H β line as

$$\text{FWHM} \approx 1.0 \times 10^3 \left(\frac{\mathcal{M}_{m_{\bullet}}^0}{10^7 M_{\odot}}\right)^{1/2} \left(\frac{R_{\text{out}}}{10 \, \text{ltd}}\right)^{-1/2} \left(\frac{\mathcal{F}_R}{0.2}\right)^{1/2} \, \text{km s}^{-1}, \tag{E32}$$

from Eq. (C14). This is a typical width of the LRDs. Detailed potential, with the consideration of the sMBH disk, is complicated and depends on β_{\bullet} and γ_{\bullet} , but only weakly (varying by no more than 2/3: Huré & Hersant 2011), thereby shaping the profile of the broad H β line. Currently, the cMBH masses are estimated by the conventional formulations of Eq. (A1) in LRDs; however, Eq. (E32) implies that the mass estimates (Maiolino et al. 2024b) for the cMBHs are actually close to the total masses of the sMBHs and the cMBHs (negligible compared with $\mathcal{M}_{m_{\bullet}}$).

The presence of the sMBHs makes it hard to measure the cMBH masses unless the central regions can be spatially resolve. Even the most powerful GRAVITY+/VLTI is unable to measure the CMBH, but future Kilometer-baseline interferometry in optical-infrared bands (Bourdarot & Eisenhauer 2024) will be capable of measuring the cMBH in local AGNs or LRD-analogs in the local universe.

F. COLLAPSE OF PRIMORDIAL CLOUDS

Theoretical considerations on CPCs were originally discussed for stars and galaxies (Hoyle 1953; Hunter 1962), subsequently for bright quasars (Field 1964) and star clusters (Peebles & Dicke 1968) in an analytical form. Nowadays, the collapse of primordial clouds has been extensively studied by numerical simulations for formation of star clusters (Abel et al. 2000; Yoshida et al. 2003; Devecchi & Volonteri 2009), first stars (Abel et al. 2002; Bromm et al. 2002), and quasar's SMBHs (Loeb & Rasio 1994). However, publications about CPCs as the origin of quasars in the 1960s have gradually faded into the obscurity of historical literature. Notwithstanding, these heuristic ideas may prove valuable for understanding the present LRDs in light of the collapsing structure, in particular, the CPC structure of a core with an envelope (Unno et al. 1967; Matsuda & Satō 1969; Hirasawa 1969). The characteristic structures provide a compelling picture of the LRD's absorption features of $H\alpha$ and $H\beta$ lines.

Details of the CPCs are far beyond the scope of this paper, but we hope to grasp the radiative acceleration of the envelope for the absorption features of LRDs. For the simplest discussion, we assume a homogeneous gas sphere with a density of ρ_c . While nuclear starburst is triggered during the collapse (Field 1964), the radiation pressure of the starburst will push a gaseous envelope with a radius of D_{en} to expand outward. The kinetic energy of the envelope is given by

$$\frac{1}{2}M_{\rm en}V_{\rm en}^2 = \eta_* f_* M_{\rm core} c^2 \tau_{\rm abs},\tag{F33}$$

where $M_{\rm en}$ is the envelope mass with absorption optical depth $\tau_{\rm abs}$, $V_{\rm en}$ is the velocity, $M_{\rm core}$ is the nuclear starburst mass, η_* is the converting efficiency of the nuclear reaction and f_* is the star formation efficiency. We have the typical velocity of

$$V_{\rm en} = 112.2 \,\eta_{7}^{1/2} f_{-2}^{1/2} \tau_{0.1}^{1/2} q_{-2}^{1/2} \,\mathrm{km} \,\mathrm{s}^{-1}, \tag{F34}$$

where $\eta_7 = \eta_*/0.007$, $f_{-2} = f_*/10^{-2}$ and $q_{-2} = q/10^{-2}$ and $q = M_{\rm core}/M_{\rm en}$ is the mass ratio of the core to the envelope. This corresponds to a distance to the center

$$D_{\rm en} \approx 4.3 \, M_7 V_{100}^{-2} \, \rm pc,$$
 (F35)

from $V_{\rm en}^2 = G\left(M_{\bullet} + \mathscr{M}_{m_{\bullet}}\right)/D_{\rm en}$, where $M_7 = \left(M_{\bullet} + \mathscr{M}_{m_{\bullet}}\right)/10^7\,M_{\odot}$ and $V_{100} = V_{\rm en}/100\,{\rm km~s^{-1}}$.

Considering that the envelope is composed of $\mathcal{N}_{\rm cl}$ clumps, we have the covering factor $\mathcal{C} = \mathcal{N}_{\rm cl} r_{\rm cl}^2/D_{\rm sh}^2$, where $r_{\rm cl}$ is the radius of individual clumps in the envelope. Mass conservation for the envelope gives $\mathcal{N}_{\rm cl}\rho_{\rm cl}r_{\rm cl}^3 = D_{\rm en}^3\rho_{\rm c}$. We have the optical depth of individual clouds as

$$\tau_{\rm abs} = \kappa_{\rm abs} \rho_{\rm cl} r_{\rm cl} = 0.2 \, C_{0.1}^{-1} \kappa_{-2} \rho_{-19} D_{\rm sh, 5},$$
 (F36)

where $\kappa_{-2} = \kappa_{\rm abs}/10^{-2}$, $\rho_{-19} = \rho_{\rm c}/10^{-19}\,{\rm g\,cm^{-3}}$, $D_{\rm sh,5} = D_{\rm sh}/5\,{\rm pc}$, and $C_{0.1} = C/0.1$, a value indicated by the fraction of the LRDs with absorption features. The existence of such a thin absorbing layer is the result of the interaction between the core and the outflowing envelope. This simple estimation of the envelope agrees with the absorption features of the Balmer lines.

Finally, we would point out that the LRD-analogs in the local universe provide interesting comparisons. The LRDs mostly appear in the early universe (Ma et al. 2025) though there are a few local analogs (Lin et al. 2025a,b; Chen et al. 2025a; Ji et al. 2025b). J 1025+1402 (z=0.1) shows extremely high equivalent width NaD, K I, Fe II, and Ca II triplet absorption lines (Lin et al. 2025b; Ji et al. 2025b). Another object, J 204837.26-002437.2 (z=0.4), shows a star formation rate of $400\,M_\odot\,\mathrm{yr}^{-1}$ in extended star formation regions (Chen et al. 2025a). However, how are the high-z LRDs similar to these local analogs remains an open question.

G. FITTING SCHEME

G.1. LRD samples

We began by collecting all LRD sources reported in previous studies (Kocevski et al. 2025; Setton et al. 2024). After cross-matching these catalogs and removing duplicates, we obtained a unified list of LRDs. We then searched for the corresponding JWST/NIRSpec spectra of these sources in the DAWN JWST Archive (DJA; https://dawn-cph.github.io/dja/). The DJA is a public database maintained by the DAWN Initiative, providing uniformly processed NIRSpec and NIRCam data from major extragalactic surveys such as CEERS, JADES, and PRIMER. Among the compiled candidates, those with available NIRSpec/PRISM spectra were selected for analysis. Tab. 2 lists three representative kinds of LRDs with PRISM spectroscopy identified in the DJA. The PRISM configuration offers a broad, continuous wavelength coverage from $0.6 \,\mu\text{m}$ to $5.3 \,\mu\text{m}$ at low spectral resolution ($R \approx 100$), enabling simultaneous measurement of the mid-infrared continuum. The three kinds of LRDs characterize the global spectral energy distribution of LRDs.

 $F_{\lambda, {\rm AMS}}$ and $F_{\lambda, {\rm MBH}}$ are obtained by the model described by Eq. (6) in Appendix C. Continuum from nuclear starbursts can be obtained by CIGALE (Boquien et al. 2019). The emission from a starburst depends on its age, initial mass function and total mass. In this paper, we use CIGALE to fit the Balmer part to obtain an approximate continuum of starbursts (f_{λ}). Using a normalization α_0 for the starburst continuum, we jointly fit the SEDs with the s@cMBH-disk. We define

$$\chi^2 = \sum_{i=1}^{N} \frac{1}{\sigma_i^2} \left(F_{\lambda}^{\text{obs},i} - F_{\lambda,\text{AMS}}^i - F_{\lambda,\text{MBH}}^i - F_{\lambda,\text{NSB}}^i \right)^2, \tag{G37}$$

where $F_{\lambda, \text{NSB}}^i = \alpha_0 f_{\lambda}^i$, and σ_i are the observational errors. We mask the emission lines in the fitting. The fitting results are obtained when χ^2 reaches its minimum.

Ji et al. (2025c) found that GN-z11 ($z\approx 10.6$) has an excess between $0.3-0.35\,\mu\mathrm{m}$ remains open. Here we propose that this is similar to the rest-frame optical continuum of LRDs contributed by the s@cMBH-disk, but $\mathcal{R}_{\mathrm{in}}$ will be much smaller than in typical LRDs. This scenario can be tested by monitoring campaigns if this component is variable.

REFERENCES

Abel, T., Bryan, G. L., & Norman, M. L. 2000, ApJ, 540, 39, —. 2002, Science, 295, 93, doi: 10.1126/science.1063991

- Abramowicz, M. A., Czerny, B., Lasota, J. P., & Szuszkiewicz, E. 1988, ApJ, 332, 646, doi: 10.1086/166683
- Akins, H. B., Casey, C. M., Chisholm, J., et al. 2025, arXiv e-prints, arXiv:2503.00998, doi: 10.48550/arXiv.2503.00998
- Amaro-Seoane, P., Andrews, J., Arca Sedda, M., et al. 2023, Living Reviews in Relativity, 26, 2, doi: 10.1007/s41114-022-00041-y
- Ananna, T. T., Bogdán, Á., Kovács, O. E., Natarajan, P., & Hickox,R. C. 2024, arXiv e-prints, arXiv:2404.19010,doi: 10.48550/arXiv.2404.19010
- Arcodia, R., Merloni, A., Nandra, K., et al. 2021, Nature, 592, 704, doi: 10.1038/s41586-021-03394-6
- Arcodia, R., Liu, Z., Merloni, A., et al. 2024, A&A, 684, A64, doi: 10.1051/0004-6361/202348881
- Baggen, J. F. W., van Dokkum, P., Labbé, I., et al. 2023, ApJL, 955, L12, doi: 10.3847/2041-8213/acf5ef
- Barkana, R., & Loeb, A. 2001, PhR, 349, 125, doi: 10.1016/S0370-1573(01)00019-9
- Barnes, J., & Efstathiou, G. 1987, ApJ, 319, 575, doi: 10.1086/165480
- Bentz, M. C., Denney, K. D., Grier, C. J., et al. 2013, ApJ, 767, 149, doi: 10.1088/0004-637X/767/2/149
- Billand, J.-B., Elbaz, D., Gentile, F., et al. 2025, arXiv e-prints, arXiv:2507.04011, doi: 10.48550/arXiv.2507.04011
- Blandford, R. D., & McKee, C. F. 1982, ApJ, 255, 419, doi: 10.1086/159843
- Boquien, M., Burgarella, D., Roehlly, Y., et al. 2019, A&A, 622, A103, doi: 10.1051/0004-6361/201834156
- Bourdarot, G., & Eisenhauer, F. 2024, arXiv e-prints, arXiv:2410.22063, doi: 10.48550/arXiv.2410.22063
- Bromm, V., Coppi, P. S., & Larson, R. B. 2002, ApJ, 564, 23, doi: 10.1086/323947
- Carranza-Escudero, M., Conselice, C. J., Adams, N., et al. 2025, ApJL, 989, L50, doi: 10.3847/2041-8213/adf73d
- Casey, C. M., Akins, H. B., Kokorev, V., et al. 2024, arXiv e-prints, arXiv:2407.05094, doi: 10.48550/arXiv.2407.05094
- Casey, C. M., Akins, H. B., Finkelstein, S. L., et al. 2025, arXiv e-prints, arXiv:2505.18873, doi: 10.48550/arXiv.2505.18873
- Cenci, E., & Habouzit, M. 2025, MNRAS, 542, 2597, doi: 10.1093/mnras/staf1362
- Chakraborty, J., Kara, E., Masterson, M., et al. 2021, ApJL, 921, L40, doi: 10.3847/2041-8213/ac313b
- Chen, X., Ichikawa, K., Akiyama, M., et al. 2025a, arXiv e-prints, arXiv:2510.02801, doi: 10.48550/arXiv.2510.02801
- Chen, Y.-M., Wang, J.-M., Yan, C.-S., Hu, C., & Zhang, S. 2009, ApJL, 695, L130, doi: 10.1088/0004-637X/695/2/L130
- Chen, Y.-X., Jiang, Y.-F., & Goodman, J. 2025b, arXiv e-prints, arXiv:2505.13951, doi: 10.48550/arXiv.2505.13951
- Chen, Y.-X., Jiang, Y.-F., Goodman, J., & Lin, D. N. C. 2024, ApJ, 974, 106, doi: 10.3847/1538-4357/ad6dd4

- Cheng, K. S., & Wang, J.-M. 1999, ApJ, 521, 502, doi: 10.1086/307572
- Choi, J.-H., Shlosman, I., & Begelman, M. C. 2013, ApJ, 774, 149, doi: 10.1088/0004-637X/774/2/149
- Chokshi, A., & Turner, E. L. 1992, MNRAS, 259, 421, doi: 10.1093/mnras/259.3.421
- de Graaff, A., Brammer, G., Weibel, A., et al. 2025, A&A, 697, A189, doi: 10.1051/0004-6361/202452186
- D'Eugenio, F., Maiolino, R., Perna, M., et al. 2025, arXiv e-prints, arXiv:2503.11752, doi: 10.48550/arXiv.2503.11752
- Devecchi, B., & Volonteri, M. 2009, ApJ, 694, 302, doi: 10.1088/0004-637X/694/1/302
- Di Giovanni, M. 2025, arXiv e-prints, arXiv:2505.11033, doi: 10.48550/arXiv.2505.11033
- Du, P., & Wang, J.-M. 2019, ApJ, 886, 42, doi: 10.3847/1538-4357/ab4908
- Du, P., Hu, C., Lu, K.-X., et al. 2014, ApJ, 782, 45, doi: 10.1088/0004-637X/782/1/45
- Eisenstein, D. J., & Loeb, A. 1995, ApJ, 443, 11, doi: 10.1086/175498
- Eisenstein, D. J., Willott, C., Alberts, S., et al. 2023, arXiv e-prints, arXiv:2306.02465, doi: 10.48550/arXiv.2306.02465
- Fan, X., & Wu, Q. 2023, ApJ, 944, 159, doi: 10.3847/1538-4357/acb532
- Ferrarese, L., Côté, P., Dalla Bontà, E., et al. 2006, ApJL, 644, L21, doi: 10.1086/505388
- Field, G. B. 1964, ApJ, 140, 1434, doi: 10.1086/148048
- Frank, J., King, A., & Raine, D. J. 2002, Accretion Power in Astrophysics: Third Edition
- Gilbaum, S., & Stone, N. C. 2022, ApJ, 928, 191, doi: 10.3847/1538-4357/ac4ded
- Giustini, M., Miniutti, G., & Saxton, R. D. 2020, A&A, 636, L2, doi: 10.1051/0004-6361/202037610
- Graham, M. J., Ford, K. E. S., McKernan, B., et al. 2020, PhRvL, 124, 251102, doi: 10.1103/PhysRevLett.124.251102
- Graham, M. J., McKernan, B., Ford, K. E. S., et al. 2023, ApJ, 942, 99, doi: 10.3847/1538-4357/aca480
- Greene, J. E., & Ho, L. C. 2005, ApJ, 630, 122, doi: 10.1086/431897
- Greene, J. E., Labbe, I., Goulding, A. D., et al. 2024, ApJ, 964, 39, doi: 10.3847/1538-4357/ad1e5f
- Haas, M., Klaas, U., Müller, S. A. H., et al. 2003, A&A, 402, 87, doi: 10.1051/0004-6361:20030110
- Hirasawa, T. 1969, Progress of Theoretical Physics, 42, 523, doi: 10.1143/PTP.42.523
- Hoyle, F. 1953, ApJ, 118, 513, doi: 10.1086/145780
- Hubeny, I. 1990, ApJ, 351, 632, doi: 10.1086/168501
- Hunter, C. 1962, ApJ, 136, 594, doi: 10.1086/147410
- Huré, J. M., & Hersant, F. 2011, A&A, 531, A36, doi: 10.1051/0004-6361/201015854

- Hviding, R. E., de Graaff, A., Miller, T. B., et al. 2025, A&A, 702, A57, doi: 10.1051/0004-6361/202555816
- Inayoshi, K., & Ichikawa, K. 2024, ApJL, 973, L49, doi: 10.3847/2041-8213/ad74e2
- Inayoshi, K., & Maiolino, R. 2025, ApJL, 980, L27, doi: 10.3847/2041-8213/adaebd
- Jahnke, K. 2025, The Open Journal of Astrophysics, 8, 9, doi: 10.33232/001c.129063
- Ji, X., Maiolino, R., Übler, H., et al. 2025a, arXiv e-prints, arXiv:2501.13082, doi: 10.48550/arXiv.2501.13082
- Ji, X., D'Eugenio, F., Juodžbalis, I., et al. 2025b, arXiv e-prints, arXiv:2507.23774, doi: 10.48550/arXiv.2507.23774
- Ji, X., Maiolino, R., Ferland, G., et al. 2025c, MNRAS, 541, 2134, doi: 10.1093/mnras/staf1083
- Juodžbalis, I., Marconcini, C., D'Eugenio, F., et al. 2025a, arXiv e-prints, arXiv:2508.21748, doi: 10.48550/arXiv.2508.21748
- Juodžbalis, I., Maiolino, R., Baker, W. M., et al. 2025b, arXiv e-prints, arXiv:2504.03551, doi: 10.48550/arXiv.2504.03551
- Kaspi, S., Smith, P. S., Netzer, H., et al. 2000, ApJ, 533, 631, doi: 10.1086/308704
- Kato, S., Fukue, J., & Mineshige, S., eds. 1998, Black-hole accretion disks
- Kocevski, D. D., Finkelstein, S. L., Barro, G., et al. 2025, ApJ, 986, 126, doi: 10.3847/1538-4357/adbc7d
- Kokorev, V., Caputi, K. I., Greene, J. E., et al. 2024, ApJ, 968, 38, doi: 10.3847/1538-4357/ad4265
- Kritos, K., & Silk, J. 2025, arXiv e-prints, arXiv:2510.21709, doi: 10.48550/arXiv.2510.21709
- Labbé, I., van Dokkum, P., Nelson, E., et al. 2023, Nature, 616, 266, doi: 10.1038/s41586-023-05786-2
- Labbe, I., Greene, J. E., Bezanson, R., et al. 2025, ApJ, 978, 92, doi: 10.3847/1538-4357/ad3551
- Lambrides, E., Garofali, K., Larson, R., et al. 2024, arXiv e-prints, arXiv:2409.13047, doi: 10.48550/arXiv.2409.13047
- Larson, R. B. 1969, MNRAS, 145, 271, doi: 10.1093/mnras/145.3.271
- Leung, G. C. K., Finkelstein, S. L., Pérez-González, P. G., et al. 2024, arXiv e-prints, arXiv:2411.12005, doi: 10.48550/arXiv.2411.12005
- Li, J., Silverman, J. D., Shen, Y., et al. 2025, ApJ, 981, 19, doi: 10.3847/1538-4357/ada603
- Lin, R., Zheng, Z.-Y., Jiang, C., et al. 2025a, ApJL, 980, L34, doi: 10.3847/2041-8213/adaaf1
- Lin, X., Fan, X., Cai, Z., et al. 2025b, arXiv e-prints, arXiv:2507.10659, doi: 10.48550/arXiv.2507.10659
- Lin, X., Fan, X., Wang, F., et al. 2025c, arXiv e-prints, arXiv:2504.08039, doi: 10.48550/arXiv.2504.08039
- Liu, H., Jiang, Y.-F., Quataert, E., Greene, J. E., & Ma, Y. 2025, arXiv e-prints, arXiv:2507.07190,
 - doi: 10.48550/arXiv.2507.07190

- Loeb, A. 1993, ApJ, 403, 542, doi: 10.1086/172224
- Loeb, A., & Rasio, F. A. 1994, ApJ, 432, 52, doi: 10.1086/174548
- Lu, K.-X., Huang, Y.-K., Zhang, Z.-X., et al. 2019, ApJ, 877, 23, doi: 10.3847/1538-4357/ab16e8
- Luo, J., An, H., Bian, L., et al. 2025, arXiv e-prints, arXiv:2502.20138, doi: 10.48550/arXiv.2502.20138
- Luo, Y., & Wang, J.-M. 2025, MNRAS, doi: 10.1093/mnras/staf841
- Ma, Y., Greene, J. E., Volonteri, M., et al. 2025, arXiv e-prints, arXiv:2509.02662, doi: 10.48550/arXiv.2509.02662
- Magorrian, J., Tremaine, S., Richstone, D., et al. 1998, AJ, 115, 2285, doi: 10.1086/300353
- Maiolino, R., Scholtz, J., Curtis-Lake, E., et al. 2024a, A&A, 691, A145, doi: 10.1051/0004-6361/202347640
- Maiolino, R., Scholtz, J., Witstok, J., et al. 2024b, Nature, 627, 59, doi: 10.1038/s41586-024-07052-5
- Marconi, A., Risaliti, G., Gilli, R., et al. 2004, MNRAS, 351, 169, doi: 10.1111/j.1365-2966.2004.07765.x
- Masterson, M., Kara, E., Panagiotou, C., et al. 2025, Nature, 638, 370, doi: 10.1038/s41586-024-08385-x
- Matsuda, T., & Satō, H. 1969, Progress of Theoretical Physics, 41, 1021, doi: 10.1143/PTP.41.1021
- Matthee, J., Naidu, R. P., Brammer, G., et al. 2024, ApJ, 963, 129, doi: 10.3847/1538-4357/ad2345
- McKernan, B., Ford, K. E. S., Lyra, W., et al. 2011, MNRAS, 417, L103, doi: 10.1111/j.1745-3933.2011.01132.x
- Mineshige, S., Kawaguchi, T., Takeuchi, M., & Hayashida, K. 2000, PASJ, 52, 499, doi: 10.1093/pasj/52.3.499
- Miniutti, G., Saxton, R. D., Giustini, M., et al. 2019, Nature, 573, 381, doi: 10.1038/s41586-019-1556-x
- Mo, H., van den Bosch, F. C., & White, S. 2010, Galaxy Formation and Evolution, doi: 10.1017/CBO9780511807244
- Naidu, R. P., Matthee, J., Katz, H., et al. 2025, arXiv e-prints, arXiv:2503.16596, doi: 10.48550/arXiv.2503.16596
- Netzer, H. 2009, MNRAS, 399, 1907,
 - doi: 10.1111/j.1365-2966.2009.15434.x
- Neumayer, N., Seth, A., & Böker, T. 2020, A&A Rv, 28, 4, doi: 10.1007/s00159-020-00125-0
- Pacucci, F., & Narayan, R. 2024, ApJ, 976, 96, doi: 10.3847/1538-4357/ad84f7
- Peebles, P. J. E. 1969, ApJ, 155, 393, doi: 10.1086/149876
- Peebles, P. J. E., & Dicke, R. H. 1968, ApJ, 154, 891, doi: 10.1086/149811
- Pérez-González, P. G., Barro, G., Rieke, G. H., et al. 2024, ApJ, 968, 4, doi: 10.3847/1538-4357/ad38bb
- Pizzati, E., Hennawi, J. F., Schaye, J., et al. 2025, MNRAS, 539, 2910, doi: 10.1093/mnras/staf660
- Rees, M. J. 1984, ARA&A, 22, 471,
 - doi: 10.1146/annurev.aa.22.090184.002351

- Rinaldi, P., Bonaventura, N., Rieke, G. H., et al. 2024, arXiv e-prints, arXiv:2411.14383, doi: 10.48550/arXiv.2411.14383
- Ross, R. R., Fabian, A. C., & Mineshige, S. 1992, MNRAS, 258, 189, doi: 10.1093/mnras/258.1.189
- Rusakov, V., Watson, D., Nikopoulos, G. P., et al. 2025, arXiv e-prints, arXiv:2503.16595, doi: 10.48550/arXiv.2503.16595
- Setton, D. J., Greene, J. E., de Graaff, A., et al. 2024, arXiv e-prints, arXiv:2411.03424, doi: 10.48550/arXiv.2411.03424
- Setton, D. J., Greene, J. E., Spilker, J. S., et al. 2025, arXiv e-prints, arXiv:2503.02059, doi: 10.48550/arXiv.2503.02059
- Shakura, N. I., & Sunyaev, R. A. 1973, A&A, 24, 337
- Shimura, T., & Takahara, F. 1993, ApJ, 419, 78, doi: 10.1086/173460
- Sirko, E., & Goodman, J. 2003, MNRAS, 341, 501, doi: 10.1046/j.1365-8711.2003.06431.x
- Sołtan, A. 1982, MNRAS, 200, 115, doi: 10.1093/mnras/200.1.115
- Tagawa, H., Haiman, Z., & Kocsis, B. 2020, ApJ, 898, 25, doi: 10.3847/1538-4357/ab9b8c
- Taylor, A. J., Kokorev, V., Kocevski, D. D., et al. 2025, arXiv e-prints, arXiv:2505.04609, doi: 10.48550/arXiv.2505.04609
- Tee, W. L., Fan, X., Wang, F., & Yang, J. 2025, ApJL, 983, L26, doi: 10.3847/2041-8213/adc5e3
- The LIGO Scientific Collaboration, the Virgo Collaboration, & the KAGRA Collaboration. 2025, arXiv e-prints, arXiv:2507.08219. https://arxiv.org/abs/2507.08219
- Unno, W., Kato, S., & Osaki, Y. 1967, ZA, 65, 327
- Vaccaro, M. P., Seif, Y., & Mapelli, M. 2025, arXiv e-prints, arXiv:2508.03637, doi: 10.48550/arXiv.2508.03637
- Vanzella, E., Calura, F., Meneghetti, M., et al. 2019, MNRAS, 483, 3618, doi: 10.1093/mnras/sty3311
- Volonteri, M., & Rees, M. J. 2005, ApJ, 633, 624, doi: 10.1086/466521
- Wang, B., Leja, J., Labbé, I., et al. 2024, ApJS, 270, 12, doi: 10.3847/1538-4365/ad0846
- Wang, J.-M., Du, P., Baldwin, J. A., et al. 2012, ApJ, 746, 137, doi: 10.1088/0004-637X/746/2/137
- Wang, J.-M., Liu, J.-R., Ho, L. C., & Du, P. 2021a, ApJL, 911, L14, doi: 10.3847/2041-8213/abee81
- Wang, J.-M., Liu, J.-R., Ho, L. C., Li, Y.-R., & Du, P. 2021b, ApJL, 916, L17, doi: 10.3847/2041-8213/ac0b46
- Wang, J.-M., Liu, J.-R., Li, Y.-R., et al. 2023a, ApJL, 958, L40, doi: 10.3847/2041-8213/ad0bd9

- Wang, J.-M., Watarai, K.-Y., & Mineshige, S. 2004, ApJL, 607, L107, doi: 10.1086/421906
- Wang, J.-M., Yan, C.-S., Gao, H.-Q., et al. 2010, ApJL, 719, L148, doi: 10.1088/2041-8205/719/2/L148
- Wang, J.-M., & Zhou, Y.-Y. 1999, ApJ, 516, 420, doi: 10.1086/307080
- Wang, J.-M., Ge, J.-Q., Hu, C., et al. 2011, ApJ, 739, 3, doi: 10.1088/0004-637X/739/1/3
- Wang, J.-M., Du, P., Hu, C., et al. 2014, ApJ, 793, 108, doi: 10.1088/0004-637X/793/2/108
- Wang, J.-M., Zhai, S., Li, Y.-R., et al. 2023b, ApJ, 954, 84, doi: 10.3847/1538-4357/acdf48
- Wang, J.-M., Hu, C., Chen, Y.-J., et al. 2025a, arXiv e-prints, arXiv:2511.07716. https://arxiv.org/abs/2511.07716
- Wang, Y.-L., Liu, J.-R., & Wang, J.-M. 2025b, A&A, 695, A143, doi: 10.1051/0004-6361/202452114
- Woosley, S. E., Heger, A., & Weaver, T. A. 2002, Reviews of Modern Physics, 74, 1015, doi: 10.1103/RevModPhys.74.1015
- Xu, Z.-H., Chen, Y.-X., & Lin, D. N. C. 2025, arXiv e-prints, arXiv:2511.03904. https://arxiv.org/abs/2511.03904
- Yoshida, N., Abel, T., Hernquist, L., & Sugiyama, N. 2003, ApJ, 592, 645, doi: 10.1086/375810
- Yoshioka, S., Mineshige, S., Ohsuga, K., Kawashima, T., & Kitaki, T. 2024, PASJ, 76, 1015, doi: 10.1093/pasj/psae067
- Yu, Q., & Tremaine, S. 2002, MNRAS, 335, 965, doi: 10.1046/j.1365-8711.2002.05532.x
- Yue, M., Eilers, A.-C., Ananna, T. T., et al. 2024, ApJL, 974, L26, doi: 10.3847/2041-8213/ad7eba
- Zhang, C., Wu, Q., Fan, X., et al. 2025a, arXiv e-prints, arXiv:2505.12719, doi: 10.48550/arXiv.2505.12719
- Zhang, Z., Jiang, L., Liu, W., & Ho, L. C. 2024, arXiv e-prints, arXiv:2411.02729, doi: 10.48550/arXiv.2411.02729
- Zhang, Z., Jiang, L., Liu, W., Ho, L. C., & Inayoshi, K. 2025b, arXiv e-prints, arXiv:2506.04350, doi: 10.48550/arXiv.2506.04350
- Zhou, S., Sun, M., Liu, T., et al. 2024, ApJL, 966, L9, doi: 10.3847/2041-8213/ad3c3f
- Zhuang, M.-Y., Li, J., Shen, Y., et al. 2025, arXiv e-prints, arXiv:2505.20393, doi: 10.48550/arXiv.2505.20393
- Zwick, L., Tiede, C., & Mayer, L. 2025, arXiv e-prints, arXiv:2507.22014, doi: 10.48550/arXiv.2507.22014

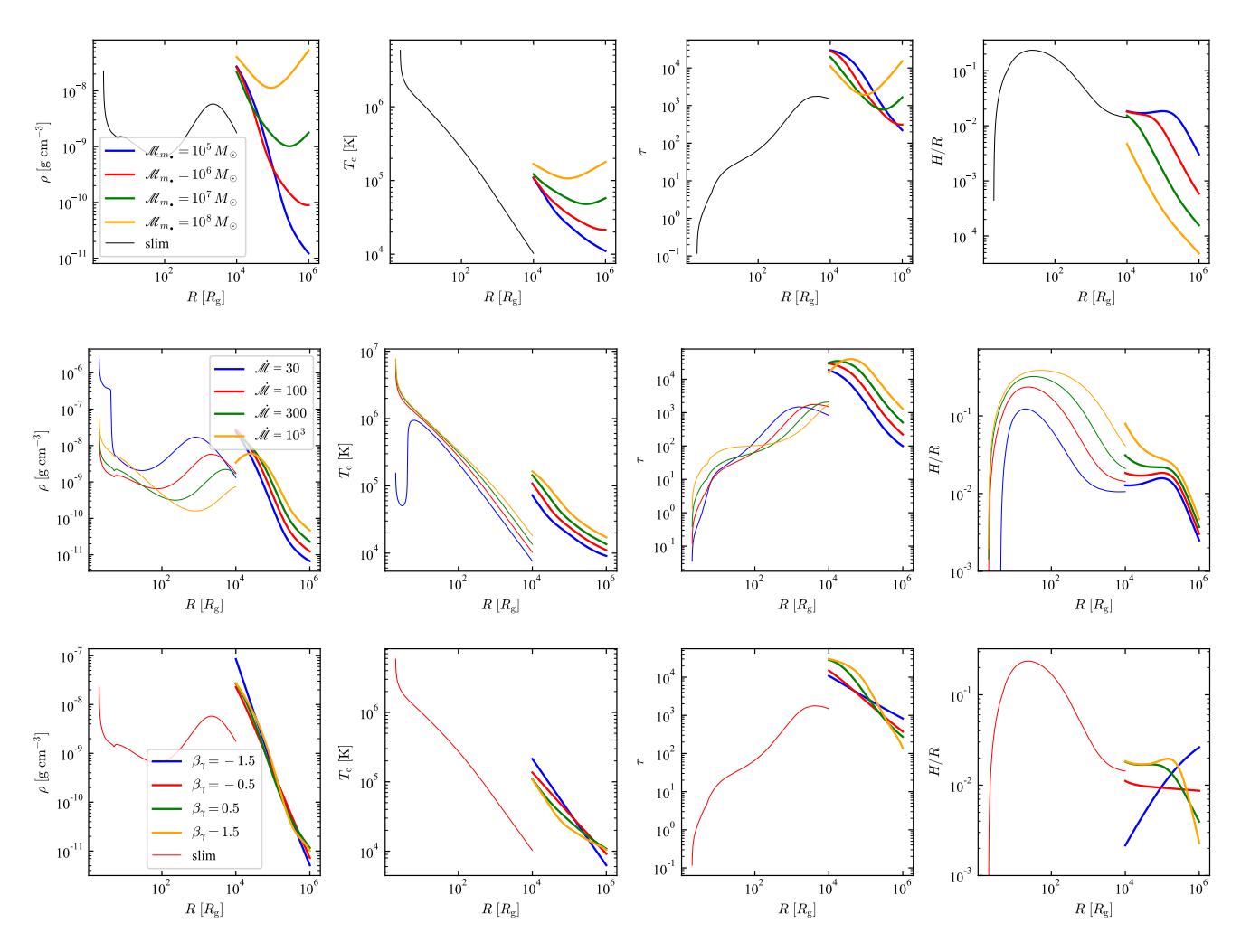


Figure 5. Radial profiles of the disk model parameters and their dependence on $\mathcal{M}_{m_{\bullet}}$, $\dot{\mathcal{M}}$, and β_{γ} . We fix the central massive black hole mass of $M_{\bullet} = 10^5 \ M_{\odot}$ for all the cases. Here $R_{\rm g} = G M_{\bullet}/c^2$ is the gravitational radius of the cMBH. The panels in the first row are for different $\mathcal{M}_{m_{\bullet}}$ and fixing $\dot{\mathcal{M}} = 100$, $\beta_{\gamma} = 1$, $\mathcal{R}_{\rm in} = 10^4 \ R_{\rm g}$, and $\mathcal{R}_{\rm out} = 10^6 \ R_{\rm g}$. The panels in the second row are for dependence of structures on different $\dot{\mathcal{M}}$. The panels in the third row are for dependence on β_{γ} .

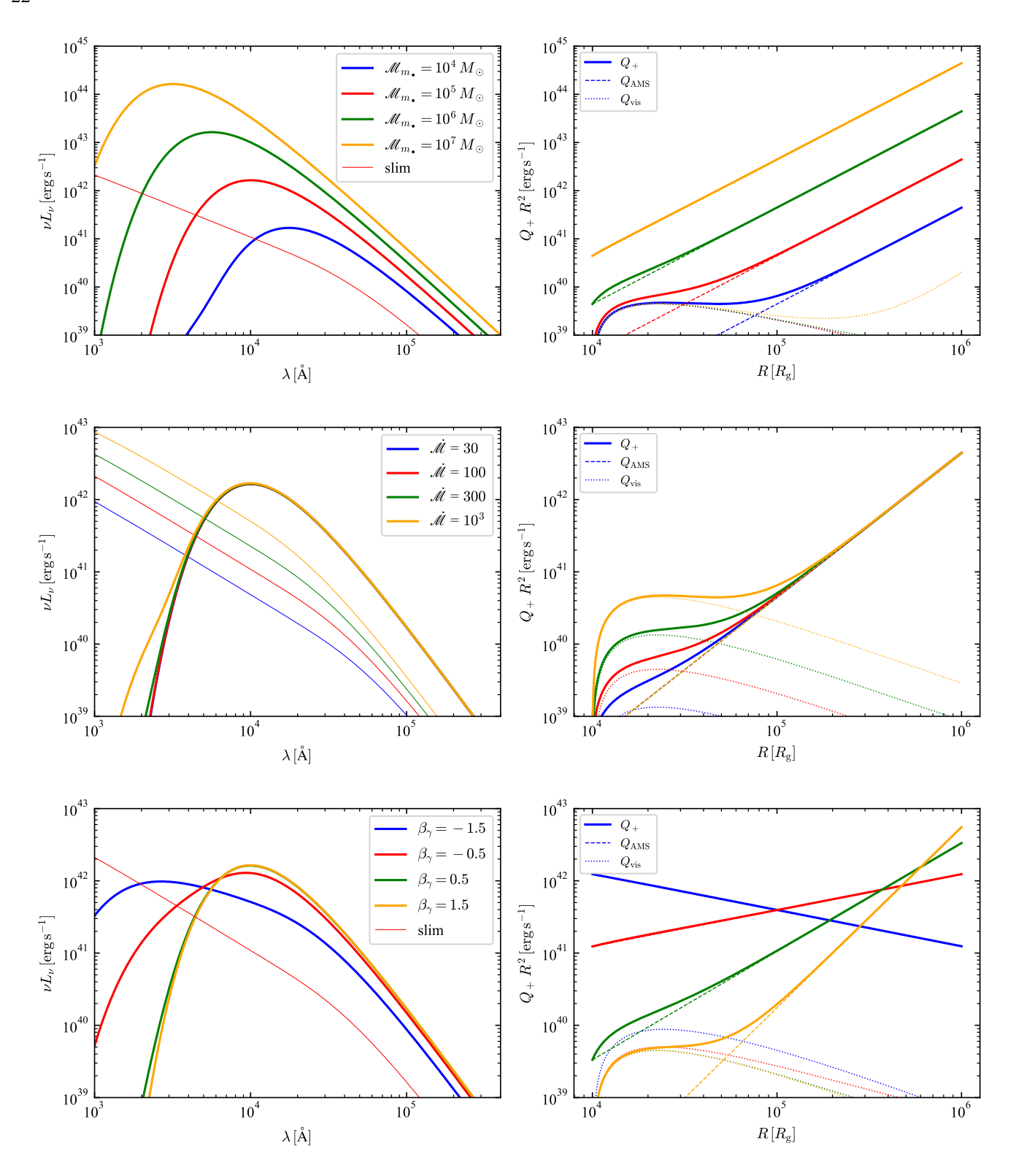


Figure 6. Comparisons of viscosity heating and AMS, and resultant SEDs, and their dependence on $\mathcal{M}_{m_{\bullet}}$, $\dot{\mathcal{M}}$, and β_{γ} . The standard parameter values are $\mathcal{M}_{m_{\bullet}} = 10^5 \, M_{\odot}$, $\dot{\mathcal{M}} = 100$, $\beta_{\gamma} = 1$, $\mathcal{R}_{\rm in} = 10^4 \, R_{\rm g}$, and $\mathcal{R}_{\rm out} = 10^6 \, R_{\rm g}$. From top to bottom, the panels correspond to variations in $\mathcal{M}_{m_{\bullet}}$, $\dot{\mathcal{M}}$, and β_{γ} , respectively.